Title: | A Pressure Relaxation Closure Model for One-Dimensional, Two-Material Lagrangian Hydrodynamics Based on the Riemann Problem

Author(s): | James Kamm, X-3 Mikhail Shashkov, T-7

Intended for: | LANL Hydro Algorithm Developers

Los Alamos
NATIONAL LABORATORY
— EST.1943 —

A Pressure Relaxation Closure Model for One-Dimensional, Two-Material Lagrangian Hydrodynamics Based on the Riemann Problem

James R. Kamm   Mikhail J. Shashkov

September 17, 2008

Contents

List of Figures

List of Tables

Abstract

Despite decades of development, Lagrangian hydrodynamics of strength-free materials presents numerous open issues, even in one dimension. We focus on the problem of closing a system of equations for a two-material cell under the assumption of a single velocity model. There are several existing models and approaches, each possessing different levels of fidelity to the underlying physics and each exhibiting unique features in the computed solutions. We consider the case in which the change in heat in the constituent materials in the mixed cell is assumed equal. An instantaneous pressure equilibration model for a mixed cell can be cast as four equations in four unknowns, comprised of the updated values of the specific internal energy and the specific volume for each of the two materials in the mixed cell. The unique contribution of our approach is for the non-instantaneous pressure relaxation case. We present a physics-inspired, geometry-based model in which the updated values of the sub-cell, relaxing-toward-equilibrium constituent pressures are related to a local Riemann problem through an optimization framework. This approach couples the modeling problem of assigning sub-cell pressures to the physics associated with the local, dynamic evolution. We package our approach in the framework of a standard predictor-corrector time integration scheme. We quantify the results of our model for idealized, two material problems using either ideal-gas or stiffened-gas equations of state.

1 Introduction

Multimaterial Lagrangian hydrodynamics of strength-free materials continues to present numerous open issues, even in one dimension. We focus on the problem of closing a system of equations for a two-material cell under the assumption of a single velocity model. We treat the constituents in these multimaterial cells as distinct, i.e., we do not consider so-called "mixture" models, often associated with multi-phase flow, in which the individual species in a computational zone are modeled as fully or partially intermingled. The unmixed, multi-material cells we consider invariably arise in multi-material Arbitrary Lagrangian-Eulerian (ALE) methods, where the results of Lagrangian hydrodynamics are projected onto a new mesh during the remap phase.

We consider three main design principles that govern closure models of

interest. The first principle is preservation of contacts; this implies that if all materials in a mixed cell are initially at the same pressure, then that pressure does not change due to the closure model. The second principle is that of pressure equilibration; that is, after some transition time (possibly only a single timestep), all pressures in the mixed cell equilibrate. The third principle is the exact conservation of total energy. As elements of such models, we assume that a separate set of material properties is maintained for each material in every multimaterial cell, together with the materials' volume fractions, which can be used to reconstruct material interfaces inside a mixed cell. The main challenge is to accurately assign the thermodynamic states of the individual material components together with the nodal forces that such a zone generates, pursuant to our design principles and despite a lack of detailed information about the velocity distribution within such cells. In particular, for the calculation of both the equation of state (EOS) and the resulting pressure forces, it is important that the calculation of the internal energy be accurate.

There are several existing models for this problem. In one class of methods (see, e.g., Barlow [4], Delov & Sadchikov [9], Goncharov & Yanilkin [11]), one estimates the velocity normal to the interface between materials and then approximates the change in the volume for each material, with internal energy updated separately for each material from its own $p\,dV$ equation. A common pressure for a mixed cell, which is used in the momentum equation, is computed using the equation of total energy conservation. Delov & Sadchikov [9] and Goncharov & Yanilkin [11] introduce an exchange of internal energy between the materials inside a mixed cell, thereby allowing some freedom in the definition of the common pressure. Other multi-material models impose either instantaneous pressure equilibration (such as that of Lagoutière [15] and Després & Lagoutière [10]) or ascribe an implicit mechanism for pressure relaxation (such as described by Tipton [26] and summarized by Shashkov [24]).

We restrict our attention to the approach in which the change in heat in the constituent materials in the mixed cell is posited to be equal, as discussed by Lagoutière [15] and Després & Lagoutière [10]. Under this assumption, the mixed-cell model can be cast as four equations in four unknowns, consisting of the updated values of the specific internal energy and the specific volume for each of the two materials in the mixed cell. A solution to this set of nonlinear equations can be obtained, e.g., with Newton's method, which forms one element of an overall predictor-corrector scheme for solving the

2

governing conservation laws.

An unsatisfactory aspect of this model, however, is the imposition of instantaneous pressure equilibration among the mixed-cell constituents. We break this assumption using a sub-cell dynamics model based on a local Riemann problem. Specifically, the unique contribution of our work is the use of this physics-inspired, geometry-based approach using an optimization framework to both (i) to break instantaneous pressure equilibration by relaxing the individual sub-cell pressures to equilibrium and (ii) to determine the single updated value of the relaxing-toward-equilibrium pressure assigned to the overall mixed cell. This approach couples the problem of assigning a single mixed-cell pressure to the physics associated with the local dynamical evolution. We discuss several test problems, using either ideal-gas or stiffened-gas equations of state, on which we exercise this method, providing complete details of the setup for each problem together with quantitative results of our approach on these problems.

This paper is structured as follows. Section 2 describes the basic 1-D Lagrangian hydrodynamics equations and the predictor-corrector scheme we employ to obtain solutions. We describe details of the two-material model, based on the work of Lagoutière [15] and Després & Lagoutière [10], in §3. Extensions of this model to account for relaxation through the dynamics of a sub-cell Riemann problem are discussed in §4. A description of test problems and results for this method is contained in §5. We summarize our findings and conclude in §6.

2   One-dimensional Lagrangian hydrodynamics

In this section, we describe the basic predictor-corrector algorithm that we use to obtain numerical solutions to the governing equations discussed in the previous section. We first restrict our attention to the single-material case, then discuss where modifications for multi-material cells are required.

The partial differential equations governing the conservation of momentum and internal energy, written in the Lagrangian frame of reference moving, are (discussed, e.g., by Caramana et al. [7]):

$$\rho\,\frac{du}{dt} + \nabla P = 0\,, \tag{1}$$

$$\rho \frac{d\varepsilon}{dt} + P \nabla \cdot u = 0 \, . \tag{2}$$

In these equations, u is the velocity and $P = P(\tau, \varepsilon)$ is the thermodynamic pressure, where ε is the specific internal energy (SIE) and τ is the specific volume, which given by the inverse of the mass density ρ of the fluid. The numerical scheme we present consists of a staggered-mesh discretization for the one-dimensional case of the above system, augmented by a trajectory equation for the cell vertices; together, this set of equations implies mass conservation. In the following, subscripts denote spatial position and superscripts associated with temporal indexing. Cell-centers (at index $i+1/2$) are associated with cell masses $M_{i+1/2}$, cell volumes $V_{i+1/2}$, and thermodynamic state variables of the cell, such as density $\rho_{i+1/2}$, specific volume $\tau_{i+1/2}$, SIE $\varepsilon_{i+1/2}$, pressure $p_{i+1/2}$, and sound speed $cs_{i+1/2}$. The vertices of cell i are associated with edge positions x_i and x_{i+1}, edge velocities u_i and u_{i+1}, and node-centered control volume masses m_i and m_{i+1}.

We assume that we have all the necessary information to completely specify the values of all state variables at time t^n and seek to update the solution to time $t^{n+1} \equiv t^n + \delta t$, where δt is the timestep chosen to satisfy necessary stability requirements (e.g., the CFL condition). The following set of coupled, implicit equations capture the dynamics of the one-dimensional conservation equations by linking the updated values of the flowfield with the current state:

$$m_i \frac{u_i^{n+1} - u_i^n}{\delta t} = -\Delta \left(\frac{p_i^n + p_i^{n+1}}{2} \right) \, , \tag{3}$$

$$u_i^{n+1/2} = \frac{1}{2} \left(u_i^n + u_i^{n+1} \right) \, , \tag{4}$$

$$x_i^{n+1} = x_i^n + \delta t \cdot u_i^{n+1/2} \, , \tag{5}$$

$$V_{i+1/2}^{n+1} = x_{i+1}^{n+1} - x_i^{n+1} \, , \tag{6}$$

$$\tau_{i+1/2}^{n+1} = V_{i+1/2}^{n+1} / M_{i+1/2} \, , \tag{7}$$

$$M_{i+1/2} \frac{\varepsilon_{i+1/2}^{n+1} - \varepsilon_{i+1/2}^n}{\delta t} = - \left(\frac{p_{i+1/2}^n + p_{i+1/2}^{n+1}}{2} \right) \Delta^* u_{i+1/2}^{n+1/2} \, , \tag{8}$$

$$p_{i+1/2}^{n+1} = \mathcal{P}(\tau_{i+1/2}^{n+1}, \varepsilon_{i+1/2}^{n+1}) \, . \tag{9}$$

Here, $\mathcal{P}$ is the mapping that gives the pressure as a function of the density and SIE. Also, the operator Δ and its adjoint Δ^* are defined on the appropriate

4

discrete function spaces as:

$$\Delta \xi_i \equiv \xi_{i+1/2} - \xi_{i-1/2} \,, \tag{10}$$

$$\Delta^* \eta_{i+1/2} \equiv \eta_{i+1} - \eta_i \,. \tag{11}$$

We propose the following iterative scheme by which to obtain a solution for the variables at t^{n+1} in Eqs. (3)–(9):

$$\text{Set} \quad p_{i+1/2}^{n+1,0} := p_{i+1/2}^n \quad \text{and iterate for } s = 1, \dots : \tag{12}$$

$$m_i \, \frac{u_i^{n+1,s} - u_i^n}{\delta t} = -\Delta \left(\frac{p_i^n + p_i^{n+1,s-1}}{2} \right) , \tag{13}$$

$$u_i^{n+1/2,s} = \frac{1}{2} \left(u_i^n + u_i^{n+1,s} \right) , \tag{14}$$

$$x_i^{n+1,s} = x_i^n + \delta t \cdot u_i^{n+1/2,s} , \tag{15}$$

$$V_{i+1/2}^{n+1,s} = x_{i+1}^{n+1,s} - x_i^{n+1,s} , \tag{16}$$

$$\tau_{i+1/2}^{n+1,s} = V_{i+1/2}^{n+1,s} / M_{i+1/2} , \tag{17}$$

$$M_{i+1/2} \, \frac{\varepsilon_{i+1/2}^{n+1,s} - \varepsilon_{i+1/2}^n}{\delta t} = - \left(\frac{p_{i+1/2}^n + p_{i+1/2}^{n+1,s-1}}{2} \right) \Delta^* u_{i+1/2}^{n+1/2,s} , \tag{18}$$

$$p_{i+1/2}^{n+1,s} = \mathcal{P}(\tau_{i+1/2}^{n+1,s}, \varepsilon_{i+1/2}^{n+1,s}) . \tag{19}$$

As shown by Bauer et al. [5], this iteration is stable under the usual constraints, e.g., CFL number between zero and one. Moreover, this scheme is nominally second order accurate in both space and time for sufficiently smooth initial conditions and sufficiently short times; the method invariably degenerates to first order as discontinuous flow features develop.

One can interpret the first two iterations of this algorithm as a predictor-corrector method. We write this numerical scheme as follows:

Predictor

$$m_i \, \frac{u_i^{n+1,\star} - u_i^n}{\delta t} = -\Delta \left(p_i^n \right) , \tag{20}$$

$$\Rightarrow \quad u_i^{n+1,\star} = u_i^n - \frac{\delta t}{m_i} \left(p_{i+1/2}^n - p_{i-1/2}^n \right) , \tag{21}$$

$$u_i^{n+1/2,\star} = \frac{1}{2} \left(u_i^n + u_i^{n+1,\star} \right) , \tag{22}$$

5

$$x_i^{n+1,\star} = x_i^n + \delta t \cdot u_i^{n+1/2,\star}, \tag{23}$$

$$V_{i+1/2}^{n+1,\star} = x_{i+1}^{n+1,\star} - x_i^{n+1,\star}, \tag{24}$$

$$\tau_{i+1/2}^{n+1,\star} = V_{i+1/2}^{n+1,\star} / M_{i+1/2}, \tag{25}$$

$$M_{i+1/2} \frac{\varepsilon_{i+1/2}^{n+1,\star} - \varepsilon_{i+1/2}^n}{\delta t} = -p_{i+1/2}^n \Delta^* u_{i+1/2}^{n+1/2,\star}, \tag{26}$$

$$\Rightarrow \quad \varepsilon_{i+1/2}^{n+1,\star} = \varepsilon_{i+1/2}^n - \frac{\delta t}{M_{i+1/2}} p_{i+1/2}^n \left(u_{i+1}^{n+1/2,\star} - u_i^{n+1/2,\star} \right), \tag{27}$$

$$p_{i+1/2}^{n+1,\star} = \mathcal{P}(\tau_{i+1/2}^{n+1,\star}, \varepsilon_{i+1/2}^{n+1,\star}). \tag{28}$$

<p align="center">Corrector</p>

$$m_i \frac{u_i^{n+1} - u_i^n}{\delta t} = -\Delta \left(\frac{p_i^n + p_i^{n+1,\star}}{2} \right), \tag{29}$$

$$\Rightarrow \quad u_i^{n+1} = u_i^n - \frac{1}{2} \frac{\delta t}{m_i} \left(p_{i+1/2}^n + p_{i+1/2}^{n+1,\star} - p_{i-1/2}^n - p_{i-1/2}^{n+1,\star} \right), \tag{30}$$

$$u_i^{n+1/2} = \frac{1}{2} \left(u_i^n + u_i^{n+1} \right), \tag{31}$$

$$x_i^{n+1} = x_i^n + \delta t \cdot u_i^{n+1/2}, \tag{32}$$

$$V_{i+1/2}^{n+1} = x_{i+1}^{n+1} - x_i^{n+1}, \tag{33}$$

$$\tau_{i+1/2}^{n+1} = V_{i+1/2}^{n+1} / M_{i+1/2}, \tag{34}$$

$$M_{i+1/2} \frac{\varepsilon_{i+1/2}^{n+1} - \varepsilon_{i+1/2}^n}{\delta t} = -\left(\frac{p_{i+1/2}^n + p_{i+1/2}^{n+1,\star}}{2} \right) \Delta^* u_{i+1/2}^{n+1/2}, \tag{35}$$

$$\Rightarrow \quad \varepsilon_{i+1/2}^{n+1} = \varepsilon_{i+1/2}^n - \frac{1}{2} \frac{\delta t}{M_{i+1/2}} \left(p_{i+1/2}^n + p_{i+1/2}^{n+1,\star} \right)$$
$$\times \left(u_{i+1}^{n+1/2} - u_i^{n+1/2} \right), \tag{36}$$

$$p_{i+1/2}^{n+1} = \mathcal{P}(\tau_{i+1/2}^{n+1}, \varepsilon_{i+1/2}^{n+1}). \tag{37}$$

This two-step scheme can be made more efficient and equally as accurate (at least formally) by replacing the EOS call in Eq. (28) with a predictor pressure assignment based on an adiabatic relation among pressure, density, and SIE. In this case, we replace Eq. (28) by:

$$p_{i+1/2}^{n+1,\star} = p_{i+1/2}^n - \frac{(cs_{i+1/2}^n)^2}{\tau_{i+1/2}^n} \frac{\delta V_{i+1/2}^{n+1,\star}}{V_{i+1/2}^n}, \tag{38}$$

where $\delta V_{i+1/2}^{n+1,\star} \equiv V_{i+1/2}^{n+1,\star} - V_{i+1/2}^n$. One must, however, retain the full EOS call in the corrector step of Eq. (37), to ensure thermodynamic consistency and conservation at the updated time.

To decrease non-physical results for problems with nominally C^0 solutions (e.g., shockwaves), the pressure in these expressions must be augmented by an artificial viscosity to provide additional numerical dissipation. In practice, we modify each occurrence of the pressure p in the above approach by adding an additional term q: notionally, $p_{i+1/2} \leftarrow p_{i+1/2} + q_{i+1/2}$ in Eqs. (3), (8), etc. For example, to calculate the artificial viscosity $q_{i+1/2}^n$ at cell centers at t^n, used in Eqs. (21) and (27), the classical linear-plus-quadratic model of von Neumann & Richtmyer [28] (see also Landshoff [16]), active only in compression, is evaluated as:

$$q_{i+1/2}^n = \begin{cases} 0\,, & \text{if } u_{i+1}^n - u_i^n \geq 0, \\ -\nu_1\, \rho_{i+1/2}^n\, cs_{i+1/2}^n\, (u_{i+1}^n - u_i^n) + \nu_2\, \rho_{i+1/2}^n\, (u_{i+1}^n - u_i^n)^2\,, & \text{otherwise}, \end{cases}$$

(39)

where ν_1 (numerically, nominally ~ 1) and ν_2 (~ 0.1) are the coefficients of the linear and quadratic contributions, respectively, and $\rho_{i+1/2}^n \equiv 1/\tau_{i+1/2}^n$. Similar expressions apply to predictor values of artificial viscosity, used, e.g., in Eqs. (30) and (36). While more sophisticated artificial viscosity models are available (as described, e.g., by Campbell & Shashkov [6]), the simple linear-plus-quadratic model is sufficient to demonstrate the efficacy of the numerical methods for the 1-D gasdynamics problems discussed here.

3   Two-Material Instantaneous Equilibration Model

We now examine a specific instantaneous pressure equilibrium model for a two-material mixed cell. We make the fundamental assumption that the fluids are not intermingled; that is, we assume that there is a scale on which the two fluids are separated. We first review the model based on the work of Lagoutière [15] and Després & Lagoutière [10] and discuss how to use this model with the above algorithm.

A schematic of the mixed cell is shown in Fig. 1, which indicates material 1 to the left of an idealized (massless) interface, which separates it from material 2 to the right. In the following discussion, we largely suppress the subscript index of the mixed cell, i_{mix}; instead, subscripts refer to the two

materials in the multi-material cell. In keeping with the single-material algorithm discussed in the previous section, assume that we have the following quantities, consistently updated to time t^{n+1}:

1. τ^{n+1}: the updated value of the overall specific volume of the mixed cell, from Eqs. (25) and (34); and

2. ε^{n+1}: the updated value of the overall SIE of the mixed cell, from Eqs. (27) and (36).

We also know a common pressure at the previous timestep, p^n, for the mixed cell; we discuss later how to update this common pressure from the constituent materials' updated pressures. In addition to those values, we know the specific volume and SIE of the mixed cell's constituent materials at the previous timestep, i.e., τ_1^n, τ_2^n, ε_1^n, ε_2^n.

The quantities that we seek are the updated values of these properties, viz.,

1. τ_1^{n+1}, τ_2^{n+1}: the updated specific volumes of materials 1 and 2, and

2. ε_1^{n+1}, ε_2^{n+1}: the updated SIEs of materials 1 and 2.

With these values, the individual materials' EOSs define the associated thermodynamic variables. In the mixed cell, denote the mass fractions ("concentrations") by c_1 and c_2 for materials 1 and 2, respectively:

$$c_1 = m_1/M_{i_\mathrm{mix}} \quad \text{and} \quad c_2 = m_2/M_{i_\mathrm{mix}}, \tag{40}$$

where in the mixed cell

$$m_1 = \text{mass of material 1}, \quad m_2 = \text{mass of material 2}, \tag{41}$$
$$M_{i_\mathrm{mix}} = \text{total mass} = m_1 + m_2. \tag{42}$$

Since the masses in the Lagrangian cells are fixed, the mass fractions c_1 and c_2 do not vary with time.

The governing equations of the closure model discussed by Lagoutière [15] and Després & Lagoutière [10] are the following.

- Conservation of mass (expressed with the specific volume):

$$c_1\tau_1^{n+1} + c_2\tau_2^{n+1} = \tau^{n+1}. \tag{43}$$

- Conservation of internal energy (expressed with the SIE):

$$c_1 \varepsilon_1^{n+1} + c_2 \varepsilon_2^{n+1} = \varepsilon^{n+1} \, . \tag{44}$$

- Equality of change in heat of the two materials: with $dQ_k = d\varepsilon_k + P_k \, dV_k$, this requirement implies:

$$\varepsilon_1^{n+1} - \varepsilon_1^n + P_1(\tau_1^{n+1} - \tau_1^n) = \varepsilon_2^{n+1} - \varepsilon_2^n + P_2(\tau_2^{n+1} - \tau_2^n) \, . \tag{45}$$

- Equality of thermodynamic pressure $\mathcal{P}_k(\tau, \varepsilon)$ of the two materials ($k = 1,2$):[1]

$$p = p_1^{n+1} = p_2^{n+1} \quad \Rightarrow \quad \mathcal{P}_1(\tau_1^{n+1}, \varepsilon_1^{n+1}) - \mathcal{P}_2(\tau_2^{n+1}, \varepsilon_2^{n+1}) = 0 \, . \tag{46}$$

The four relations (43), (44),[2] (45), and (46) form a set of four nonlinear equations in four unknowns: τ_1^{n+1}, ε_1^{n+1}, τ_2^{n+1}, and ε_2^{n+1}.

A choice must be made in how to model the pressure in Eq. (45). Among the obvious options are the following (where $k = 1,2$ for the two materials):

- *"Fully Implicit"*: $P_k = p_k^{n+1}$, the pressure at the updated time;

- *"Fully Explicit"*: $P_k = p_k^n$, the pressure at the previous time; or

- *"Thermodynamically Consistent"*: $P_k = \frac{1}{2}\left(p_k^n + p_k^{n+1}\right)$, the arithmetic mean of the previous-time and updated-time pressures.

For a polytropic gas, closed-form solutions of this set of equations can be obtained in each of these three cases. In Appendix A, we provide these solutions to Eqs. (43)–(46) for polytropic gases. Many of these expressions are algebraically very involved, but nevertheless comprise a useful result with which one can verify the software implementation of the algorithm.

For general EOSs, Eqs. (43)–(46) do not admit a closed-form solution, whether one considers the fully implicit, fully explicit, or thermodynamically consistent closure models. We now describe an approach with which to implement Newton's method to obtain numerical solutions of these coupled equations. First, rewrite these equations in the form

$$\boldsymbol{f}(\boldsymbol{x}) = \boldsymbol{0} \, , \tag{47}$$

---

[1] This relation explicitly specifies the common pressure of the mixed cell.

[2] As explained by Després & Lagoutière [10], Eqs. (43) and (44) are consistent with the assumption that the fluids are separated at some scale.

where

$$\boldsymbol{x} \equiv \left[\tau_1^{n+1},\, \varepsilon_1^{n+1},\, \tau_2^{n+1},\, \varepsilon_2^{n+1}\right]^T, \tag{48}$$

$$\boldsymbol{f} \equiv [f_1,\, f_2,\, f_3,\, f_4]^T, \tag{49}$$

with the components of f corresponding to the model equations:

$$f_1 \equiv c_1\tau_1^{n+1} + c_2\tau_2^{n+1} - \tau^{n+1}, \tag{50}$$

$$f_2 \equiv c_1\varepsilon_1^{n+1} + c_2\varepsilon_2^{n+1} - \varepsilon^{n+1}, \tag{51}$$

$$f_3 \equiv \varepsilon_1^{n+1} - \varepsilon_1^n + P_1(\tau_1^{n+1} - \tau_1^n)$$
$$\quad - \left[\varepsilon_2^{n+1} - \varepsilon_2^n + P_2(\tau_2^{n+1} - \tau_2^n)\right]. \tag{52}$$

$$f_4 \equiv \mathcal{P}_1(\tau_1^{n+1}, \varepsilon_1^{n+1}) - \mathcal{P}_2(\tau_2^{n+1}, \varepsilon_2^{n+1}), \tag{53}$$

A simple implementation of Newton's method for the system in Eq. (47) can be written as:

$$\boldsymbol{x}^{\nu+1} = \boldsymbol{x}^\nu - \beta \cdot \delta\boldsymbol{x}^\nu \quad \text{for } \nu = 0, \dots, \text{ where} \tag{54}$$

$$\delta\boldsymbol{x}^\nu = \left(\frac{\partial \boldsymbol{f}}{\partial \boldsymbol{x}}\right)^{-1}_{\boldsymbol{x}^k} \boldsymbol{f}(\boldsymbol{x}^k), \tag{55}$$

with $\beta \in (0, 1]$ being a value that scales the magnitude of the Newton step.

The elements of the Jacobian matrix $\partial\boldsymbol{f}/\partial\boldsymbol{x}$ are given by

$$\left(\frac{\partial \boldsymbol{f}}{\partial \boldsymbol{x}}\right)_{ij} \equiv \frac{\partial f_i}{\partial x_j}. \tag{56}$$

The 4×4 matrix $\partial\boldsymbol{f}/\partial\boldsymbol{x}$ has several zero elements in the first two rows. The modeling choice for the pressure term P_k in Eq. (52) affects the specific form of the Jacobian elements:

- "*Fully Implicit*": $P_k = p_k^{n+1} = \mathcal{P}_k(\tau_2^{n+1}, \varepsilon_2^{n+1})$, which depends on the unknown vector $\boldsymbol{x}$.

- "*Fully Explicit*": $P_k = p_k^n$, independent of the unknown vector $\boldsymbol{x}$.

- "*Thermodynamically Consistent*": this model uses the arithmetic mean of the previous two models, $P_k = \frac{1}{2}\left(p_k^n + p_k^{n+1}\right) = \frac{1}{2}\left(p_k^n + \mathcal{P}_k(\tau_2^{n+1}, \varepsilon_2^{n+1})\right)$, which also depends on the unknown vector $\boldsymbol{x}$.

10

Expressions for the elements of the Jacobian are given in Appendix B. These expressions can be used in software implementations of the Newton's method iteration.[3]

To initialize the iteration in Eqs. (54) and (55), the initial values for the unknowns are taken to be those at time t^n:

$$\boldsymbol{x}^0 = [\tau_1^n,\, \varepsilon_1^n,\, \tau_2^n,\, \varepsilon_2^n]^T \ . \tag{57}$$

This iteration was found to converge rapidly for the cases considered in §5.

4   Two-Material Riemann Problem/Pressure Relaxation Model

The model of the previous section provides an approach in which the pressures of the constituents of a two-material cell are equilibrated at the end of each timestep. In this section, we describe a sub-cell dynamics model that leads naturally to schemes by which to relax the constituent pressures to equilibrium. That is, given an initial state with a discrepancy between the pressures of material 1 and material 2, we seek a model with which to update material pressures p_1^{n+1} and p_2^{n+1} such that the difference between these values approaches zero as time increases.[4] We do so with a purely dynamical model that does not appeal to any explicit dissipation terms, per se.

To set the stage for this model, the relaxation operator $\mathcal{R}$ takes as input the thermodynamic states of the constituent materials at time t^n together with values for the overall specific volume and SIE at time t^{n+1}. On output, the thermodynamic states of the individual materials are updated to time t^{n+1} and some estimate of an updated common cell pressure is provided. Schematically, we write this as:

$$\mathcal{R}\left(\tau_1^n, \varepsilon_1^n, \tau_2^n, \varepsilon_2^n; \tau^{n+1}, \varepsilon^{n+1}\right) = \left\{\tau_1^{n+1}, \varepsilon_1^{n+1}, \tau_2^{n+1}, \varepsilon_2^{n+1}; p_1^{n+1}, p_2^{n+1}, p^{n+1}\right\} \ . \tag{58}$$

In this section we describe in detail the relaxation operator $\mathcal{R}$.

---

[3]To accelerate this algorithm, one could perform a small number of iterations in the Newton step, instead of converging the solution.

[4]This idealized picture is for the special case of stationary flow, i.e., in the absence of external flow perturbations. More generally, there will be external flow effects and, so, one should not expect pressure equilibration in a mixed cell to necessarily obtain.

4.1 Two-Material Riemann-Problem/Relaxation Model: Equations

The foundation of this approach is to consider the evolution of the multi-material cell over one timestep to be related to a local Riemann problem. This cell is identified by the index i_{mix}, with the states of the two materials assumed to be available at time t^n. The location of the interface between the materials at this time determined by the local volume fraction of, say, material 1, given by f_1:

$$x^n_{\mathrm{intfc}} = x^n_{i_{\mathrm{mix}}} + f_1(x^n_{i_{\mathrm{mix}}+1} - x^n_{i_{\mathrm{mix}}}) \in \left[x^n_{i_{\mathrm{mix}}}, x^n_{i_{\mathrm{mix}}+1}\right]. \tag{59}$$

Specifically, the two states in this cell at t^n are given by:

$$(\rho, e, p, u) = \begin{cases} \left(\rho_1, e_1, p_1, u_{i_{\mathrm{mix}}}\right) , & \text{if } x^n_{i_{\mathrm{mix}}} < x < x^n_{\mathrm{intfc}} , \\ \left(\rho_2, e_2, p_2, u_{i_{\mathrm{mix}}+1)}\right) , & \text{if } x^n_{\mathrm{intfc}} < x < x^n_{i_{\mathrm{mix}}+1} . \end{cases} \tag{60}$$

The solution to this one-cell Riemann problem problem at time t^{n+1} can be computed for polytropic gases according to the method of Gottlieb & Groth [12], for stiffened gases following Plohr [21], and for more general equations of state as described by Colella & Glaz [8] and Quartapelle et al. [22].

A schematic of the initial conditions and idealized solution to this problem is shown in Fig. 2, which depicts the pressure for the mixed cell at t^n on the bottom and at t^{n+1} on the top, in the particular case of a rarefaction-contact-shock configuration. In this figure, the top (t^{n+1}) diagram exhibits, from left to right, the left t^n state, the leading left-most Riemann wave (W^L), the contact discontinuity (W^*), the leading right-most Riemann wave (W^R), and the right t^n state. We emphasize that the states outside of the leading waves are unchanged from their values at t^n during the timestep δt. If the left- or right-most wave is a shock, then the precise location of this wave is unambiguous; if this wave is a rarefaction, however, then we do not use the exact solution but instead choose either the head or tail of the rarefaction as defining the location of this wave (as in Fig. 2). In the domains delimited by these waves, i.e., between the left-most wave and the contact, and between the contact and the right-most wave, we assume the Riemann-problem pressure is constant in space at time t^{n+1}; outside these waves, we assume that the pressure retains its initial (i.e., at t^n) values. Depending on the initial conditions of the Riemann problem, these assumptions may not

be strictly valid (e.g., when rarefactions are present); nonetheless, they can be used in the optimization method that we describe below.[5]

Let the region to the left of the contact contain two sets Ω_1 and Ω_2, defined as

$$\Omega_1 \equiv \left\{ x : x_{i_{\mathrm{mix}}}^{n+1} < x < x_{\mathrm{left}}^{\mathrm{RP}} \right\} \quad \text{and} \quad \Omega_2 \equiv \left\{ x : x_{\mathrm{left}}^{\mathrm{RP}} < x < x_{\mathrm{cont}}^{\mathrm{RP}} \right\}, \quad (61)$$

where $x_{\mathrm{left}}^{\mathrm{RP}}$ is the position of the left-most wave and $x_{\mathrm{cont}}^{\mathrm{RP}}$ is the contact position, both determined from the solution to the Riemann problem (identified by the superscript "RP"). Denote similar subsets to the right of the contact as Ω_3 and Ω_4:

$$\Omega_3 \equiv \left\{ x : x_{\mathrm{cont}}^{\mathrm{RP}} < x < x_{\mathrm{right}}^{\mathrm{RP}} \right\} \quad \text{and} \quad \Omega_4 \equiv \left\{ x : x_{\mathrm{right}}^{\mathrm{RP}} < x < x_{i_{\mathrm{mix}}+1}^{n+1} \right\}, \quad (62)$$

where $x_{\mathrm{right}}^{\mathrm{RP}}$ is the position of the right-most wave of the Riemann problem solution.

The key assumption of our approach is the following: we seek a single updated pressure values for each material (i.e., on each side of the contact) that minimizes the discrepancy between those values and the pressure given by the Riemann problem solution in that domain. A mathematical expression of this statement replaces the instantaneous pressure equilibration equation (Eq. (53) in §3) while the other constraints of the model (Eqs. (50)–(52)) still apply.

We express this relation mathematically as the following optimization problem:

$$\min_{\left\{ \tau_1^{n+1}, \varepsilon_1^{n+1}, \tau_2^{n+1}, \varepsilon_2^{n+1} \right\}} \left(||p_1^{n+1} - p_1^{\mathrm{RP}}|| + ||p_2^{n+1} - p_2^{\mathrm{RP}}|| \right) \quad (63)$$

subject to the constraints given by Eqs. (50)–(52):

$$f_1 \equiv c_1 \tau_1^{n+1} + c_2 \tau_2^{n+1} - \tau^{n+1} = 0, \quad (64)$$

$$f_2 \equiv c_1 \varepsilon_1^{n+1} + c_2 \varepsilon_2^{n+1} - \varepsilon^{n+1} = 0, \quad (65)$$

$$f_3 \equiv \varepsilon_1^{n+1} - \varepsilon_1^n + P_1 \left(\tau_1^{n+1} - \tau_1^n \right)$$
$$- \left[\varepsilon_2^{n+1} - \varepsilon_2^n + P_2 \left(\tau_2^{n+1} - \tau_2^n \right) \right] = 0. \quad (66)$$

---

[5]One could utilize the entire non-piecewise-constant solution pressure when a rarefaction fan is present. Such a model introduces additional complexity to the relaxation model presented below.

In Eq. (63), p_1^{RP} and p_2^{RP} are the solutions of the Riemann problem for the pressure in materials 1 and 2, respectively. These quantities may vary as a function of position in each of the these materials.

Using the L_2 norm, the terms in Eq. (63) can be written in terms of the locally constant pressure values in each domain:

$$||p_1^{n+1} - p_1^{\text{RP}}|| = \tilde{\Omega}_1 \left(p_1^{n+1} - p_1^{\text{RP}} \right)^2 + \tilde{\Omega}_2 \left(p_1^{n+1} - p_1^{\text{RP}} \right)^2 \quad \text{and} \quad (67)$$

$$||p_2^{n+1} - p_2^{\text{RP}}|| = \tilde{\Omega}_3 \left(p_2^{n+1} - p_2^{\text{RP}} \right)^2 + \tilde{\Omega}_4 \left(p_2^{n+1} - p_2^{\text{RP}} \right)^2 . \quad (68)$$

Here, the nondimensional quantity $\tilde{\Omega}_j$ equals the measure of the set Ω_j divided by the entire cell length, δx^{n+1}:

$$\tilde{\Omega}_j = \left(\max_{x \in \Omega_j} x - \min_{x \in \Omega_j} x \right) \Big/ \left(x_{i_{\text{mix}}+1}^{n+1} - x_{i_{\text{mix}}}^{n+1} \right) ; \quad (69)$$

with this definition,

$$\tilde{\Omega}_j \geq 0 , \ \forall j , \quad \text{and} \quad \sum_{j=1}^{4} \tilde{\Omega}_j = 1 . \quad (70)$$

Outside of the leading waves, i.e., on sets Ω_1 and Ω_4, the Riemann problem pressure equals the initial pressure:

$$p_1^{\text{RP}} = p_1^n \ \text{ for } x \in \Omega_1 \quad \text{and} \quad p_2^{\text{RP}} = p_2^n \ \text{ for } x \in \Omega_4 . \quad (71)$$

Between the contact and these waves, we assign the pressure to be the so-called "star-state" pressure of the Riemann problem solution, described, e.g., by Toro [27] and LeVeque [17]:

$$p_1^{\text{RP}} = p^* \ \text{ for } x \in \Omega_2 \quad \text{and} \quad p_2^{\text{RP}} = p^* \ \text{ for } x \in \Omega_3 . \quad (72)$$

Therefore, Eqs. (67) and (68) imply the following relations:

$$||p_1^{n+1} - p_1^{\text{RP}}|| = \tilde{\Omega}_1 \left(p_1^{n+1} - p_1^n \right)^2 + \tilde{\Omega}_2 \left(p_1^{n+1} - p^* \right)^2 \quad \text{and} \quad (73)$$

$$||p_2^{n+1} - p_2^{\text{RP}}|| = \tilde{\Omega}_3 \left(p_2^{n+1} - p^* \right)^2 + \tilde{\Omega}_4 \left(p_2^{n+1} - p_2^n \right)^2 . \quad (74)$$

We recast this constrained minimization problem as simple minimization through the use of Lagrange multipliers. Specifically, to the expression to be

14

minimized we add each of the constraint terms multiplied by an unknown parameter (the Lagrange multiplier) and then seek to minimize that composite function. The overall minimization statement then becomes the following:

$$\min_{\left\{\tau_1^{n+1}, \varepsilon_1^{n+1}, \tau_2^{n+1}, \varepsilon_2^{n+1}, \lambda_1, \lambda_2, \lambda_3\right\}} \mathcal{G}(\tau_1^{n+1}, \varepsilon_1^{n+1}, \tau_2^{n+1}, \varepsilon_2^{n+1}, \lambda_1, \lambda_2, \lambda_3) \quad (75)$$

$$\text{where} \quad \mathcal{G} \equiv ||p_1^{n+1} - p_1^{\text{RP}}|| + ||p_2^{n+1} - p_2^{\text{RP}}|| + \lambda_1 f_1 + \lambda_2 f_2 + \lambda_3 f_3 \,. \quad (76)$$

A possible extremum of the function $\mathcal{G}$ is obtained by finding a solution that corresponds to a zero of the coupled set of nonlinear equations given by:

$$\partial \mathcal{G}/\partial X_i = 0 \,, \; i = 1, \ldots, 7, \quad \text{where} \quad \boldsymbol{X} \equiv \left[\tau_1^{n+1}, \varepsilon_1^{n+1}, \tau_2^{n+1}, \varepsilon_2^{n+1}, \lambda_1, \lambda_2, \lambda_3\right]^T. \quad (77)$$

Since the derivative of $\mathcal{G}$ with respect to a Lagrange multipliers is just the corresponding constraint equation, parameter values that satisfy $\partial \mathcal{G}/\partial X_i = 0$ perforce obey the constraint equations. Numerical solutions to this problem can be sought with Newton's method for the system of equations given in Eq. (77). In this case, the elements of the function $\boldsymbol{f}$ in the Newton's method described in Eqs. (54) and (55) are comprised of the partial derivatives $\partial \mathcal{G}/\partial X_i$.

In practice, the terms in the objective function $\mathcal{G}$ are nondimensionalized by local characteristic values, so that the contributions to $\mathcal{G}$ are comparable. One such nondimensionalization is:

$$\begin{aligned}
\mathcal{G} \equiv &\; \tilde{\Omega}_1 \left(p_1^{n+1} - p_1^n\right)^2 / \bar{p}^2 + \tilde{\Omega}_2 \left(p_1^{n+1} - p^*\right)^2 / \bar{p}^2 \\
&+ \tilde{\Omega}_3 \left(p_2^{n+1} - p^*\right)^2 / \bar{p}^2 + \tilde{\Omega}_4 \left(p_2^{n+1} - p_2^n\right)^2 / \bar{p}^2 \\
&+ \lambda_1 \left[(c_1 \tau_1^{n+1} + c_2 \tau_2^{n+1})/\tau^{n+1} - 1\right] \\
&+ \lambda_2 \left[(c_1 \varepsilon_1^{n+1} + c_2 \varepsilon_2^{n+1})/\varepsilon^{n+1} - 1\right] \\
&+ \lambda_3 \left\{\left[\varepsilon_1^{n+1} - \varepsilon_1^n + P_1(\tau_1^{n+1} - \tau_1^n)\right]/\varepsilon^{n+1}\right. \\
&\quad\;\; \left. - \left[\varepsilon_2^{n+1} - \varepsilon_2^n + P_2(\tau_2^{n+1} - \tau_2^n)\right]/\varepsilon^{n+1}\right\},
\end{aligned} \quad (78)$$

where $\bar{p}$ is a characteristic pressure of the entire zone at t^n (e.g., $p_{i_{\text{mix}}}^n$).

4.2 Relaxation to a single pressure

Unlike the instantaneous pressure equilibration model, this approach does *not* imply an unambiguous value for the pressure of the mixed cell. Consistent

with the solution of the set of coupled model equations, one could assign the overall mixed-cell pressure value as a spatial average of the two updated pressures:

$$p_{i_{\text{mix}}}^{n+1} = \overline{p} = (\tilde{\Omega}_1 + \tilde{\Omega}_2)\, p_1^{n+1} + (\tilde{\Omega}_3 + \tilde{\Omega}_4)\, p_2^{n+1}\,. \qquad (79)$$

Alternatively, one could use the information from the sub-cell dynamical evolution model to assign a single pressure to the mixed cell pressure based on the extent of the wave propagation in the Riemann problem model:

$$p_{i_{\text{mix}}}^{n+1} = \tilde{p} = \tilde{\Omega}_1\, p_1^n + (\tilde{\Omega}_2 + \tilde{\Omega}_3)\, p^* + \tilde{\Omega}_4\, p_2^n\,. \qquad (80)$$

These values enter into the overall algorithm in Eqs. (21), (27), (30), and (36). In the results of §5, the common pressure given in Eq. (79) is used.

To motivate heuristically why this approach leads to pressure equilibration with increasing time, we consider the structure of the Riemann problem solutions. For polytropic gases, the four non-degenerate Riemann problem solution configurations can be denoted, following Gottlieb & Groth [12], as: RCS, RCR, SCR, and SCS, where the order corresponds to the wave family from left to right, and the letter identifies the particular wave: "R" means a rarefaction fan, "C" denotes a contact (across which the pressure equals the star-state value and is continuous), and "S" indicates a shock.[6] There are two cases: (1) the star-state pressure, p^*, is bounded by the pressures on the left and right (e.g, in the case of equal polytropic indices for the RCS and SCR solutions with no initial velocity) and (2) p^* exceeds the extremal left and right pressures (i.e., p^* is either less than the minimum pressure or greater than the maximum pressure, e.g., in the case of equal polytropic indices for the RCR and SCS solutions with no initial velocity).

Consider the first case and assume that $p_1^n < p^* < p_2^n$ (the case with $p_1^n > p^* > p_2^n$ is similar). For material 1, the result of the minimization process, p_1^{n+1}, must be bounded by p_1^n and p^*: if it were not, then one could always find a value $\tilde{p}_1^{n+1}$ that would give a smaller value of the convex combination in Eq. (73). An analogous argument holds for material 2. Thus, at the end of the timestep we have the ordering, $p_1^n < p_1^{n+1} < p^* < p_2^{n+1} < p_2^n$. Therefore, the pressure difference at the end of the timestep, $|p_1^{n+1} - p_2^{n+1}|$, is less than

---

[6]We ignore the vacuum boundary case. Additionally, the fifth case of the polytropic gas Riemann solutions is the degenerate situation in which a vacuum region develops between the opposing rarefaction waves, i.e., RCVCR, in the above notation. The consequences of this situation with respect to pressure equilibration are comparable to those of the RCR case.

the pressure difference at the start of the timestep, $|p_1^n - p_2^n|$, i.e., the pressures are relaxing toward equilibrium.

Consider now the second case and assume, without loss of generality, that $p^* < p_1^n, p_2^n$; for the sake of argument, further assume that $p_1^n < p_2^n$. In material 1, the result of the minimization process, p_1^{n+1}, must again be bounded by p_1^n and p^*, and similarly for material 2: $p^* < p_1^{n+1} < p_1^n$ and $p^* < p_2^{n+1} < p_2^n$. Considering possible values of the positive numbers $\tilde{\Omega}_j$ in Eqs. (73) and (74), it is conceivable that the pressure difference could increase during the timestep (not accounting for the effect of the other constraints). Stated another way, these inequalities alone are insufficient to ensure that the pressures tend toward equilibrium, i.e., one cannot immediately infer that $|p_1^{n+1} - p_2^{n+1}| < |p_1^n - p_2^n|$. Additional special cases are those of a uniformly translating contact and a uniformly propagating shock. The former perforce obeys pressure equilibrium from t^n to t^{n+1}, while the latter necessarily maintains pressure non-equlibrium through the timestep.

Therefore, while it is plausible that some initial (i.e., t^n) mixed-cell conditions lead to a decrease in pressure difference over the course of a timestep with our model (i.e., relax toward pressure equlibrium), other initial conditions in the mixed-cell lead to the pressure difference between materials 1 and 2 increasing, at least temporarily. This (local) increase in the pressure difference between materials 1 and 2 is evident in some of the mixed-cell pressure time history results of §5; see, e.g., Fig. 11. All of the problems we consider in §5, however, lead to pressure equilibrium *at late times*. We speculate that the constituent pressures are driven, at late time, to the star-state pressure of a Riemann problem toward which the mixed cell evolves over many cycles. This speculation assumes that there are not other perturbations that enter the cell and drive it from equilibrium (such as occurs, e.g., in the problem of §5.4 and evident in Fig. 14).

4.3 2-Material Riemann-Problem/Relaxation Model: Numerical Implementation

The (single) pressure of a (two-material) mixed cell, $p_{i_{\mathrm{mix}}}^n$, where i_{mix} is the index of the mixed cell, enters into the overall algorithm, influencing the updated velocities at the edges of the mixed cell. Therefore, the manner in which an overall pressure for the multi-material mixed cell is assigned will have a direct impact on the overall results. In the predictor phase, this value

17

enters in the evaluation of the predictor velocity $u_i^{n+1,\star}$ in Eq. (21), which influences the cell edges positions in Eq. (23), cell volumes in Eq. (24), etc., as well as in the predictor SIE in Eq. (27). Similarly, in the corrector phase, the cell velocities, edges, volumes, etc., are affected by the predictor value of the sole mixed-cell pressure in Eqs. (30)–(36). The pressures of the individual constituents in a multi-material cell are used to generate a single, overall pressure for the entire cell. In addition to this value, the updated values of the state of the two materials (viz., the specific volumes and SIEs) must be carried along into the next computational cycle.

We now describe an algorithmic implementation of the mixed cell model. As mentioned earlier, assume that we have, at time t^n, a common pressure value, $p_{i_\text{mix}}^n$, for the mixed cell as well as the thermodynamic variables for the individual constituents, τ_1^n, ε_1^n, τ_2^n, ε_2^n. In the predictor phase, the steps listed in Eqs. (20)–(27) are followed exactly, where the common pressure value from the previous timestep, $p_{i_\text{mix}}^n$, is used for the mixed cell. After the step in Eq. (27), predictor values for the overall mixed cell specific volume and SIE are generated. Instead of the single-material pressure evaluation given in Eq. (28), one invokes the mixed-cell model.

The full evaluation of the predictor values for the mixed cell is as follows.

1. Starting with the initial conditions specified by the mixed-cell state at t^n, solve the mixed-cell predictor Riemann problem over the timestep δt, which we represent notionally as $\Re(\tau_1^n, \varepsilon_1^n, \tau_2^n, \varepsilon_2^n; \delta t)$.

2. Use those results to determine the the star-state pressure and the extent of wave propagation: $\Re(\tau_1^n, \varepsilon_1^n, \tau_2^n, \varepsilon_2^n; \delta t) \Rightarrow p^*$ and $\tilde{\Omega}_j$, $j = 1, \ldots, 4$ (see Eq. (69)); these quantities are used in the evaluation of the pressure-difference expressions in Eqs. (73) and (74).

3. Obtain a solution of the associated minimization problem, given in Eqs. (75) and (76), for predictor values of the thermodynamic state of the individual constituents, $\tau_1^{n+1,\star}$, $\varepsilon_1^{n+1,\star}$, $\tau_2^{n+1,\star}$, $\varepsilon_2^{n+1,\star}$, using the values at t^n as an initial guess.

4. Evaluate the predictor component pressures with EOS calls: $p_k^{n+1,\star} = \mathcal{P}(\tau_k^{n+1,\star}, \varepsilon_k^{n+1,\star})$, $k = 1$, 2.

5. Evaluate the predictor common pressure, $p^{n+1,\star}$, according to either Eq. (79) or Eq. (80).

18

For the corrector phase, the steps listed in Eqs. (29)–(36) are followed, where the predictor common pressure value, $p^{n+1,\star}$, is now used for the mixed cell. Instead of the single-material pressure evaluation given in Eq. (37), the corrector phase of the mixed-cell model is evaluated.

1. Starting with the initial conditions specified by the mixed-cell state at t^n, solve the mixed-cell Riemann problem over the timestep δt: $\Re(\tau_1^n, \varepsilon_1^n, \tau_2^n, \varepsilon_2^n; \delta t)$.

2. Use the results of this problem to determine the star-state pressure and the extent of wave propagation: $\Re(\tau_1^n, \varepsilon_1^n, \tau_2^n, \varepsilon_2^n; \delta t) \Rightarrow p^*$ and $\tilde{\Omega}_j$, $j = 1, \ldots, 4$ (see Eq. (69)), with which one can evaluate terms of the pressure-difference expressions in Eqs. (73) and (74).

3. Solve the associated minimization problem, given in Eqs. (75) and (76), for updated values of the thermodynamic state of the individual constituents, τ_1^{n+1}, ε_1^{n+1}, τ_2^{n+1}, ε_2^{n+1}; here, the predictor values of these quantities can be used as an initial guess.

4. Evaluate the corrector component pressures with EOS calls: $p_k^{n+1} = \mathcal{P}(\tau_k^{n+1}, \varepsilon_k^{n+1})$, $k = 1, 2$.

5. Model the final common pressure, p^{n+1}, according to either Eq. (79) or Eq. (80).

5   Test Problems and Results

We now turn to several different test problems found in the compressible flow literature to evaluate the methods described above. We focus on problems with exact solutions, so that we can rigorously evaluate and compare the quantitative errors associated with different methods. While several test problems exist and are used by the single-material compressible flow algorithm development community (see, e.g., the overview by Liska & Wendroff [18]), fewer problems are available for code verification of multifluid compressible flow.

In all of the problems we consider, the mesh initially consists of N_x zones, each of identical dimension $1/(N_x + 1)$, with the exception of the central zone, which is of width $2/(N_x + 1)$. In that central zone, the mass and volume fractions are assigned to be consistent with the initial conditions,

and the initial interface between materials 1 and 2 is located in the geometric center of that cell. When Newton's method is used, we imposed an absolute L_1 convergence tolerance of at least 10^{-10} in the nondimensional test cases and 10^{-7} in the dimensional water-air shock tube problem of §5.5. For the results presented here, we assign the single mixed-cell pressure as the spatially averaged value of the two sub-cell pressures of the constituent materials, i.e., as that given in Eq. (79). We present graphical results consisting of snapshots of the computed and exact flowfields at the final time along with time-histories of the material state properties of the two materials in the multimaterial cell. Additionally, we quantify the error between the computed results and the exact solution.

5.1 The Sod Shock Tube

The Sod shock tube problem [25] is defined as the behavior of a polytropic gas with the following non-dimensional initial conditions:

$$(\gamma, \rho, e, p, u) = \begin{cases} (1.4,\ 1,\quad\ \ 2.5,\ 1,\quad 0)\ , & \text{if}\ \ 0\ \ < x < 0.5\ , \\ (1.4,\ 0.125,\ 2,\quad 0.1, 0)\ , & \text{if}\ \ 0.5 < x < 1\ , \end{cases} \tag{81}$$

with a final time of $t_{final} = 0.2$. We refer to the material to the left of $x = 0.5$ ("the interface") as "material 1" and the material to the right as "material 2." The initial condition of the mixed cell, centered at $x = 0.5$, consists of these two disparate states. The developing structure consists of a rarefaction wave moving to the left, a contact discontinuity (tracking the initial discontinuity between the two states) moving right, and a shockwave moving right (faster than the contact). The exact solution to this problem is evaluated and used to quantify the error in the computed solution.

Results of our method on this problem are shown in Figs. 3–5. Shown in Fig. 3 are, clockwise from the upper left, plots of the mass density, pressure, velocity, and SIE at the final time. These plots contain the computed values (solid line) and exact solution (dashed line) plotted against the left ordinate and the signed difference between the exact and computed results (dotted line) plotted against the right ordinate. The values corresponding to the individual material in the mixed cell are indicated with the symbol •. Errors are present at the usual locations, e.g., at the head and tail of the rarefaction and at the shock, with slight overshoots and undershoots at the contact. The SIE in Fig. 3(a) exhibits obvious overshoot on the shock-side of the contact. Table 1 catalogues the L_1 norm of the error between the computed results

20

and the exact solution for the same flow variables, evaluated pointwise on the computational domain for 100, 200, 400, and 800 zones. Also included in that table is the outcome of fitting these results to the error ansatz,

$$||y_{\text{computed}} - y_{\text{exact}}||_1 = \mathcal{A} \, \Delta x^{\sigma} \, , \tag{82}$$

where Δx is the initial, uniform mesh spacing of the problem (in all but the mixed cell). These values are depicted graphically in Fig. 4. These results suggest overall first-order convergence of the method.

Figure 5 contains time-history plots of the (from left to right) pressure, the mass density, and SIE of the two materials in the mixed cell, for the (from top to bottom) 100-, 200-, 400-, and 800-cell results. In these figures, the solid line indicates the left material (material 1) and a dotted line represents the right material (material 2). It is clear from these results that pressure equilibrium obtains for this problem by this method. Note that relaxation to equilibrium is not monotonic in the pressure difference as time progresses. Moreover, the zoning study shows that the effective relaxation effect is proportional to the mesh spacing, i.e., the time step.

5.2   The Modified Sod Shock Tube

Various authors have proposed modifications to the standard Sod shock tube problem discussed in the previous section. We consider the variant used by Shashkov [24], with the following non-dimensional initial conditions:

$$(\gamma, \rho, e, p, u) = \begin{cases} (2 \quad , 1, \quad \quad 2, 2, \quad 0) \, , & \text{if } \ 0 \ \ < x < 0.5 \, , \\ (1.4, \, 0.125, \, 2, \, 0.1, \, 0) \, , & \text{if } \ 0.5 < x < 1 \ , \end{cases} \tag{83}$$

with a final time of $t_{final} = 0.2$. As in the standard Sod case, the initial condition of the mixed cell, again centered at $x = 0.5$, contains both of these two distinct states. The solution structure is the same as the standard Sod case; however, this modified problem allows one to test the truly multimaterial aspects of our algorithm.

Results of our method on this problem are shown in Figs. 6–8. Shown in Fig. 6 are, clockwise from the upper left, plots of the mass density, pressure, velocity, and SIE at the final time. These plots contain the computed values (solid line) and exact solution (dashed line) plotted against the left ordinate and the signed difference between the exact and computed results (dotted line) plotted against the right ordinate. The values corresponding to the

21

individual material in the mixed cell are indicated with the symbol •. The stronger initial pressure difference of this problem leads to greater over- and undershoot at the shock than the standard Sod problem; as in the standard Sod results, overshoot in the shock-side SIE is seen.

Table 2 shows the L_1 norm of the error between the computed results and the exact solution for these flow variables, computed pointwise on the computational domain for 100, 200, 400, and 800 zones, together with the fit of those results to the ansatz in Eq. (82). The convergence results are slightly more uniform for this problem than for the standard Sod problem. These values are plotted in Fig. 7.

Figure 8 contains time-history plots of the (from left to right) pressure, the mass density, and SIE of the two materials in the mixed cell, for the (from top to bottom) 100-, 200-, 400-, and 800-cell results. In these figures, the solid line indicates the left material (material 1) and a dotted line represents the right material (material 2). These results are qualitatively very similar to those of the standard Sod problem, with slight non-monotonic behavior in the pressure difference, which ultimately goes to zero.

5.3   Moving Shock Problem

This problem tests the steady propagation of a shock wave in a uniform material and is used to assesses the impact of the multimaterial algorithm on the otherwise uniform flow. The non-dimensional initial conditions are:

$$(\gamma, \rho, e, p, u) = \begin{cases} (5/3,\, 4,\;\; 0.5,\quad 4/3,\qquad\quad 1)\,, & \text{if } -1 < x < 0 \,, \\ (5/3,\, 1,\; 10^{-4},\;\; 2/3{\times}10^{-4}, 0)\,, & \text{if }\quad 0 < x < 1 \,, \end{cases} \quad (84)$$

with a final time of $t_{final} = 0.5$. These initial conditions approximate an infinitely strong shock wave moving into quiescent gas at speed $u_s = 4/3$. The default mesh for this problem contains 256 cells on $-1 \leq x \leq 1$. The mixed cell is initially centered at $x = 0.0$ and contains the two states indicated above.

Results of our method on this problem are shown in Figs. 9–11. Shown in Figure 9 are, clockwise from the upper left, plots of the mass density, pressure, velocity, and SIE at the final time; again, the computed values (solid line) and exact solution (dashed line) are plotted against the left ordinate and the signed differences between these values (dotted line) are plotted against the right ordinate, with the mixed-cell values indicated by the symbol •. The perturbation in the results to the right of the origin in these plots is a

residual of the start-up error associated with the initial shock location at the origin.[7] The additional discrepancies in the solutions are associated with the contact (at $x = 0.5$) and the shock (at $x = 2/3$), where, again, over- and under-shoots occur, with the SIE overshoot being most pronounced.

Table 3 shows the L_1 norm of the error between the computed results and the exact solution for these flow variables, computed pointwise on the computational domain for 256, 512, and 1024 zones, together with the fit of those results to the ansatz in Eq. (82). These values are depicted graphically in Fig. 10. These results again suggest overall first-order convergence of the method.

Figure 11 contains time-history plots of the (from left to right) pressure, the mass density, and SIE of the two materials in the mixed cell, for the (from top to bottom) 256-, 512-, and 1024-cell results. In these figures, the solid line indicates the left material (material 1) and a dotted line represents the right material (material 2). These results present clear examples of the pressure difference converging at early time, diverging at intermediate time, and then relaxing to zero at late times. The pressure histories for this problem support the contention posited in §4.2, that the pressures computed with this model do relax to equillibrium, but in a possibly non-monotonic manner.

5.4 Shock-Contact Problem

This problem tests the transmission and reflection of a Mach 2 shock through an initially stationary contact discontinuity between two materials with disparate adiabatic indices. This problem was used by Banks et al. [3] to evaluate high-resolution Godunov algorithms for multimaterial, compressible flow in the Eulerian frame. To three significant figures, the non-dimensional initial conditions are given by:

$$(\gamma, \rho, e, p, u) = \begin{cases} (1.35,\ 2.76,\ 4.60,\ \ 4.45,\ 1.48)\ , & \text{if}\ \ 0\ \ < x < 0.1\ , \\ (1.35,\ 1.0,\ \ 2.86,\ \ 1.0,\ \ 0.0)\ , & \text{if}\ \ 0.1 < x < 0.5\ , \\ (5.0,\ \ 1.9,\ \ 0.132,\ 1.0,\ \ 0.0)\ , & \text{if}\ \ 0.5 < x < 1\ , \end{cases} \quad (85)$$

with a final time of $t_{final} = 0.25$. The default mesh for this problem has 274 cells on the initial domain $-0.37 \leq x \leq 1$. In the calculations we use high-precision initial conditions corresponding to a Mach number of two

---

[7]Evocative of this phenomenon are post-shock oscillations, as discussed by Arora & Roe [2] and LeVeque [17] for Eulerian shock capturing schemes.

corresponding to a shock speed of $u_s = 2.32$, as given in Table 4. The mixed cell is initially centered at $x = 0.5$ and contains the quiescent states of the materials with differing adiabatic indices. The shock meets this material interface at $t = 0.172$. The numerical solution for the flow state at any time can be obtained using standard shock relations (see, e.g., the report by Hurricane & Miller [13]); high-precision results for the final time are given in Table 5.

Results of our method on this problem are shown in Figs. 12–14. Shown in Fig. 12 are, clockwise from the upper left, plots of the computed (solid line) and exact (dashed line) mass density, pressure, velocity, and SIE at the final time, together with the signed difference between these values (dashed lines), as well as the mixed-cell values (●). The residual of the start-up error is evident near the origin. The reflected shock is somewhat noisier in both density and SIE than the transmitted shock, while the contact exhibits a notable undershoot in the constituent density. Table 6 catalogues the L_1 norm of the error between the computed results and the exact solution for these same flow variables, computed pointwise on the computational domain for 274, 549, 1099, and 2199 zones, together with the fit of those results to the ansatz in Eq. 82. These values are plotted in Fig. 13. These results again suggest overall first-order convergence for this problem.

Figure 14 contains time-history plots of the (from left to right) pressure, the mass density, and SIE of the two materials in the mixed cell, for the (from top to bottom) 274-, 549-, 1099-, and 2199-cell results for the initial domain $-0.37 \leq x \leq 1$. In these figures, the solid line indicates the left material (material 1) and a dotted line represents the right material (material 2). The mixed cell is initially in pressure equilibrium, which is disturbed by the passing shock, which leads to slight pressure non-equlibrium, which rapidly diminishes.

5.5 Water-Air Shock Tube

The water-air shock tube has become a standard test problem in the multimaterial compressible flow community, as it tests inherently compressible flow features, uses a slightly more complicated and stiffer EOS than the standared polytropic gas, and possesses a directly computable solution. Variations of this problem have been evaluated by several researchers, including, e.g., Andrianov [1], Johnson & Colonius [14], Luo et al. [20], and Saurel & Abgrall [23].

24

The thermodynamic properties of water in this problem are given by the stiffened-gas EOS:

$$p = (\gamma - 1) \rho e - \gamma p_\infty, \qquad (86)$$

for which the square of the sound speed is given by

$$cs^2 = \gamma (\gamma - 1) \left(e - \frac{p_\infty}{\rho} \right) = \gamma (p + p_\infty) / \rho. \qquad (87)$$

The initial conditions for this problem, in mks units, are:

$$(\gamma, p_\infty, \rho, e, p, u) = \begin{cases} (4.4,\ 6 \times 10^8,\ 10^3,\ 1.07 \times 10^6,\ 10^9,\ 0), & \text{if } 0\ \ < x < 0.7, \\ (1.4,\ 0,\qquad 50,\ 5 \times 10^4,\qquad 10^6,\ 0), & \text{if } 0.7 < x < 1, \end{cases} \qquad (88)$$

with a final time of $t_{final} = 2.2 \times 10^{-4}$ s. The multi-material cell is initially centered at $x = 0.7$ and contains the two materials specified above. The exact solution we use here is based on the solver described by Plohr [21].

Results of our method on this problem are shown in Figs. 15–17. Shown in Fig. 15 are, clockwise from the upper left, plots of the computed (solid line) and exact (dashed line) mass density, pressure, velocity, and SIE at the final time, together with the signed difference between these values (dashed lines), as well as the mixed-cell values ($\bullet$). Due to the wide dynamic range, the pressure results are depicted on a semi-log plot. Notable are the undershoot in density and overshoot in SIE at the contact; the strong rarefaction is reasonably well captured. Table 7 gives the L_1 norm of the error between the computed results and the exact solution for these flow variables, computed pointwise on the computational domain for 100, 200, 400, and 800 zones, together with the fit of those results to the ansatz in Eq. (82). These values are depicted graphically in Fig. 16. The density error on the coarsest mesh appear uncharacteristically small. Overall, these results imply first-order convergence of the method for this problem.

Figure 17 contains time-history plots of the (from left to right) pressure, the mass density, and SIE of the two materials in the mixed cell, for the (from top to bottom) 100-, 200-, 400-, and 800-cell results. In these figures, the solid line indicates the left material (material 1) and a dotted line represents the right material (material 2). The pressure difference monotonically relaxes to zero for this problem, although the pressure of material 1 is non-monotonic.

6 Summary and Conclusions

We have considered the problem of closing the system of equations for a two-material cell under the single velocity, single pressure assumption in one dimensional Lagrangian hydrodynamics. We treat the constituents in these multi-material cells as distinct, which presents the problem of how to assign the thermodynamic states of the individual material components together with the nodal forces that such a zone generates, despite a lack of detailed information within such cells. Our approach is motivated by the work of Lagoutière [15] and Després & Lagoutière [10], in which the change in heat in the constituent materials in the mixed cell is assumed to be equal. This mixed-cell model can be cast as a set of four nonlinear equations in four unknowns consisting of the updated values of the specific internal energy and the specific volume for each of the two materials in the mixed cell. A solution to this set of nonlinear equations comprises one part of an overall predictor-corrector scheme for solving the governing conservation laws.

We break the assumption of instantaneous pressure equilibration among the mixed-cell constituents in the work of Lagoutière [15] and Després & Lagoutière [10] by imposing a sub-cell dynamics model that uses a minimization problem based on a local Riemann problem. The unique contribution of our work is the use of this physics-inspired, geometry-based approach both (i) to break instantaneous pressure equilibration by relaxing the individual sub-cell pressures to equilibrium and (ii) to determine the single updated value of the relaxing-toward-equilibrium pressure assigned to the overall mixed cell. We have provided the full equations for our method as well as a description of their algorithmic implementation.

We present results of our method for several test problems, each having a directly computable solution with either ideal-gas or stiffened-gas equations of state, together complete details of the initial conditions for each problem. Quantitative evaluation of the difference between our computed results and the exact solutions demonstrates very nearly first-order convergence on each of these five problems. The mixed cell pressures in all problems evolve smoothly—but not necessarily monotonically—toward equilibrium on a timescale that decreases approximately linearly with δt. The mixed-cell solutions exhibit slight over- or undershoots in density (most noticeable in the shock-contact and water-air shocktube problems) and SIE overshoot (seen in the Sod, modified Sod, moving shock, and water-air shock tube problems).

Appendix A: Exact Solutions for Instantaneous Equilibration of Polytropic Gases

In this appendix we provide explicit formulae for the updated (t^{n+1}) thermodynamic state of the two materials in the mixed cell assuming instantaneous pressure equilibration. These results are solutions of Eqs. (43)–(46). We provide closed-form solutions for four approaches: (1) the closed-form solution of Loubère et al. [19] (which we refer to as the LSDL model), (2) the "fully implicit" model, (3) the "fully explicit" model, and (4) the "thermodynamically consistent" model. These expressions can be used in both the predictor and corrector phases of the algorithm presented above.

A.1 The LSDL Model

The LSDL model [19] assumes both materials are described by a polytropic EOS, with possibly different adiabatic indices. The assumption here is equivalent to the "fully implicit" model. In [19], Loubère et al. present a compact form of the exact solution. For this result, define the parameters:

$$D = c_1\,\gamma_1 + c_2\,\gamma_2\,, \quad a = \varepsilon_1^n - \varepsilon_2^n\,, \quad b = \tau_1^n - \tau_2^n\,, \tag{A1}$$

$$\alpha_1 = (\gamma_2\,\varepsilon^{n+1} + c_2\,a)/D\,, \quad \alpha_2 = (\gamma_1\,\varepsilon^{n+1} - c_1\,a)/D\,, \tag{A2}$$

$$\beta_1 = c_2\,b/D\,, \quad \beta_2 = -c_1\,b/D\,. \tag{A3}$$

Loubère et al. show that the closed-form expression for the overall mixed cell pressure is given by

$$p^{n+1} = \left[c_1\,(\gamma_1 - 1)\,\alpha_1 + c_2\,(\gamma_2 - 1)\,\alpha_2\right] / \\ \left[\tau^{n+1} - c_1\,(\gamma_1 - 1)\,\beta_1 - c_2\,(\gamma_2 - 1)\,\beta_2\right]\,. \tag{A4}$$

From this quantity, the mixed cell constituent specific volume and SIE are given as:

$$\tau_1^{n+1} = (\gamma_1 - 1)\left[(\alpha_1/p^{n+1}) + \beta_1\right]\,, \tag{A5}$$

$$\tau_2^{n+1} = (\gamma_2 - 1)\left[(\alpha_2/p^{n+1}) + \beta_2\right]\,, \tag{A6}$$

$$\varepsilon_1^{n+1} = \alpha_1 + \beta_1\,p^{n+1}\,, \tag{A7}$$

$$\varepsilon_2^{n+1} = \alpha_2 + \beta_2\,p^{n+1}\,. \tag{A8}$$

With these values, the associated properties of the constituents of the mixed cell can be evaluated.

A.2 The Fully Implicit Model

In the "*Fully Implicit*" approach, the pressures in Eq. (46) are given by $P_1 = p_1^{n+1}$ and $P_2 = p_2^{n+1}$. This is equivalent to the assumptions of the LDSL [19] model of the previous section. As an alternative to those results, symbolic manipulation software was used to obtain closed-form expressions for the solution in this case. One must distinguish between the case of identical gases (i.e., $\gamma_1 = \gamma_2 \equiv \gamma$) and that of non-identical gases (i.e., $\gamma_1 \neq \gamma_2$).

A.2.1 Fully implicit, identical gases

When $\gamma_1 = \gamma_2 \equiv \gamma$, the solution is given as:

$$p = (\gamma - 1)\, \varepsilon^{n+1}/\tau^{n+1} \,, \tag{A9}$$

$$\varepsilon_1^{n+1} = \frac{\gamma\, \varepsilon^{n+1}\tau^{n+1} + c_2\left[(\gamma - 1)\left(\tau_1^n - \tau_2^n\right)\varepsilon^{n+1} + \left(\varepsilon_1^n - \varepsilon_2^n\right)\tau^{n+1}\right]}{\gamma\left(c_1 + c_2\right)\tau^{n+1}} \,, \tag{A10}$$

$$\varepsilon_2^{n+1} = \frac{\gamma\, \varepsilon^{n+1}\tau^{n+1} - c_1\left[(\gamma - 1)\left(\tau_1^n - \tau_2^n\right)\varepsilon^{n+1} + \left(\varepsilon_1^n - \varepsilon_2^n\right)\tau^{n+1}\right]}{\gamma\left(c_1 + c_2\right)\tau^{n+1}} \,, \tag{A11}$$

$$\tau_1^{n+1} = \frac{\gamma\, \varepsilon^{n+1}\tau^{n+1} + c_2\left[(\gamma - 1)\left(\tau_1^n - \tau_2^n\right)\varepsilon^{n+1} + \left(\varepsilon_1^n - \varepsilon_2^n\right)\tau^{n+1}\right]}{\gamma\left(c_1 + c_2\right)\varepsilon^{n+1}} \,, \tag{A12}$$

$$\tau_2^{n+1} = \frac{\gamma\varepsilon^{n+1}\tau^{n+1} - c_1\left[(\gamma - 1)\left(\tau_1^n - \tau_2^n\right)\varepsilon^{n+1} + \left(\varepsilon_1^n - \varepsilon_2^n\right)\tau^{n+1}\right]}{\gamma\left(c_1 + c_2\right)\varepsilon^{n+1}} \,. \tag{A13}$$

A.2.2 Fully implicit, non-identical identical gases

When $\gamma_1 \neq \gamma_2$, the solution is given as:

$$p = \frac{c_1 c_2\left(\gamma_1 - \gamma_2\right)\left(\varepsilon_1^n - \varepsilon_2^n\right) + \left[c_1\gamma_2\left(\gamma_1 - 1\right) + c_2\gamma_1\left(\gamma_2 - 1\right)\right]\varepsilon^{n+1}}{\left(c_2\gamma_1 + c_1\gamma_2\right)\tau^{n+1} - c_1 c_2\left(\gamma_1 - \gamma_2\right)\left(\tau_1^n - \tau_2^n\right)} \tag{A14}$$

$$\varepsilon_1^{n+1} = \frac{\gamma_2\varepsilon^{n+1}\tau^{n+1} + c_2\left[(\gamma_2 - 1)\left(\tau_1^n - \tau_2^n\right)\varepsilon^{n+1} + \left(\varepsilon_1^n - \varepsilon_2^n\right)\tau^{n+1}\right]}{\left(c_2\gamma_1 + c_1\gamma_2\right)\tau^{n+1} - c_1 c_2\left(\gamma_1 - \gamma_2\right)\left(\tau_1^n - \tau_2^n\right)} \,, \tag{A15}$$

$$\varepsilon_2^{n+1} = \frac{\gamma_1\varepsilon^{n+1}\tau^{n+1} - c_1\left[(\gamma_1 - 1)\left(\tau_1^n - \tau_2^n\right)\varepsilon^{n+1} + \left(\varepsilon_1^n - \varepsilon_2^n\right)\tau^{n+1}\right]}{\left(c_2\gamma_1 + c_1\gamma_2\right)\tau^{n+1} - c_1 c_2\left(\gamma_1 - \gamma_2\right)\left(\tau_1^n - \tau_2^n\right)} \,, \tag{A16}$$

$$\tau_1^{n+1} = (\gamma_1 - 1)\left\{\gamma_2\,\varepsilon^{n+1}\tau^{n+1}\right.$$
$$\left. + c_2\left[(\gamma_2 - 1)\left(\tau_1^n - \tau_2^n\right)\varepsilon^{n+1} + \left(\varepsilon_1^n - \varepsilon_2^n\right)\tau^{n+1}\right]\right\}$$
$$\times \left\{\left[c_2\gamma_1\left(\gamma_2 - 1\right) + c_1\gamma_2\left(\gamma_1 - 1\right)\right]\varepsilon^{n+1} + c_1 c_2\left(\gamma_1 - \gamma_2\right)\left(\varepsilon_1^n - \varepsilon_2^n\right)\right\}^{-1} \tag{A17}$$
$$\tau_2^{n+1} = (\gamma_2 - 1)\left\{\gamma_1\,\varepsilon^{n+1}\tau^{n+1}\right.$$

$$- c_1 \left[(\gamma_1 - 1) (\tau_1^n - \tau_2^n) \, \varepsilon^{n+1} + (\varepsilon_1^n - \varepsilon_2^n) \, \tau^{n+1} \right] \}$$

$$\times \{ [c_2 \gamma_1 (\gamma_2 - 1) + c_1 \gamma_2 (\gamma_1 - 1)] \, \varepsilon^{n+1} + c_1 c_2 (\gamma_1 - \gamma_2) (\varepsilon_1^n - \varepsilon_2^n) \}^{-1} \quad \text{(A18)}$$

In the case that $|\gamma_1 - \gamma_2| \to 0$, direct algebraic manipulations show that Eqs. (A14)–(A18) reduce to the previous, equal-γ case.

A.3 The Fully Explicit Model

The "*Fully Explicit*" formulation uses $P_1 = p_1^n$ and $P_2 = p_2^n$ in Eq. (46). The algebra required to evaluate a closed-form solution is complicated, but symbolic manipulation software can be used to obtain expressions for the solution in this case. One must distinguish between the case of identical gases (i.e., $\gamma_1 = \gamma_2 \equiv \gamma$) and non-identical gases (i.e., $\gamma_1 \neq \gamma_2$). In the latter case, the solution is complicated by the fact that the pressure satisfies a quadratic equation; consequently, in that case there are two algebraically admissible solutions.

A.3.1 Fully explicit, identical gases

When $\gamma_1 = \gamma_2 \equiv \gamma$, the solution is given as:

$$p = (\gamma - 1) \, \varepsilon^{n+1} / \tau^{n+1} \,, \tag{A19}$$

$$\varepsilon_1^{n+1} = \frac{\varepsilon^{n+1} \left[\varepsilon^{n+1} + p_2^n \tau^{n+1} + c_2 \left(\varepsilon_1^n - \varepsilon_2^n + p_1^n \tau_1^n - p_2^n \tau_2^n \right) \right]}{(c_1 + c_2) \, \varepsilon^{n+1} + (c_1 p_2^n + c_2 p_1^n) \, \tau^{n+1}} \,, \tag{A20}$$

$$\varepsilon_2^{n+1} = \frac{\varepsilon^{n+1} \left[\varepsilon^{n+1} + p_1^n \tau^{n+1} - c_1 \left(\varepsilon_1^n - \varepsilon_2^n + p_1^n \tau_1^n - p_2^n \tau_2^n \right) \right]}{(c_1 + c_2) \, \varepsilon^{n+1} + (c_1 p_2^n + c_2 p_1^n) \, \tau^{n+1}} \,, \tag{A21}$$

$$\tau_1^{n+1} = \frac{\tau^{n+1} \left[\varepsilon^{n+1} + p_2^n \tau^{n+1} + c_2 \left(\varepsilon_1^n - \varepsilon_2^n + p_1^n \tau_1^n - p_2^n \tau_2^n \right) \right]}{(c_1 + c_2) \, \varepsilon^{n+1} + (c_1 p_2^n + c_2 p_1^n) \, \tau^{n+1}} \,, \tag{A22}$$

$$\tau_2^{n+1} = \frac{\tau^{n+1} \left[\varepsilon^{n+1} + p_1^n \tau^{n+1} - c_1 \left(\varepsilon_1^n - \varepsilon_2^n + p_1^n \tau_1^n - p_2^n \tau_2^n \right) \right]}{(c_1 + c_2) \, \varepsilon^{n+1} + (c_1 p_2^n + c_2 p_1^n) \, \tau^{n+1}} \,. \tag{A23}$$

A.3.2 Fully explicit, non-identical gases, first solution

When $\gamma_1 \neq \gamma_2$, one solution is given as:

$$p = \frac{1}{2} \left[(c_1 + c_2) \, \tau^{n+1} \right]^{-1}$$
$$\times \{ \quad [c_1 (\gamma_1 - 1) + c_2 (\gamma_2 - 1)] \, \varepsilon^{n+1}$$

$$- \left[c_2 \left(\gamma_1 - 1 \right) p_1^n + c_1 \left(\gamma_2 - 1 \right) p_2^n \right] \tau^{n+1}$$

$$+ c_1 c_2 \left(\gamma_1 - \gamma_2 \right) \left(\varepsilon_1^n - \varepsilon_2^n + p_1^n \tau_1^n - p_2^n \tau_2^n \right)$$

$$- \Big[4 c_2 \left(\gamma_1 - \gamma_2 \right) \left(\gamma_2 - 1 \right) \left(c_2 p_1^n + c_1 p_2^n \right) \tau^{n+1}$$

$$\times \left[\varepsilon^{n+1} + p_1^n \tau^{n+1} - c_1 \left(\varepsilon_1^n - \varepsilon_2^n + p_1^n \tau_1^n - p_2^n \tau_2^n \right) \right]$$

$$+ \{ - \left[c_1 \left(\gamma_1 - 1 \right) + c_2 \left(\gamma_2 - 1 \right) \right] \varepsilon^{n+1}$$

$$- \left(\gamma_2 - 1 \right) \left(c_1 p_2^n + c_2 p_1^n \right) \tau^{n+1}$$

$$+ c_2 \left(\gamma_1 - \gamma_2 \right) \left[p_1^n \tau_1^n - c_1 \left(\varepsilon_1^n - \varepsilon_2^n + p_1^n \tau_1^n - p_2^n \tau_2^n \right) \right] \}^2 \Big]^{1/2} \Big\} \quad (A24)$$

$$\varepsilon_1^{n+1} = \frac{1}{2} \left[c_1 \left(c_1 + c_2 \right) \left(\gamma_1 - \gamma_2 \right) \right]^{-1}$$

$$\times \Big\{ - \left(\gamma_2 - 1 \right) \left(c_1 + c_2 \right) \varepsilon^{n+1} - \left[c_2 \left(\gamma_1 - 1 \right) p_1^n + c_1 \left(\gamma_2 - 1 \right) p_2^n \right] \tau^{n+1}$$

$$+ c_1 \left(\gamma_1 - \gamma_2 \right) \left[\varepsilon^{n+1} + c_2 \left(\varepsilon_1^n - \varepsilon_2^n + p_1^n \tau_1^n - p_2^n \tau_2^n \right) \right]$$

$$- \Big[4 c_2 \left(\gamma_1 - \gamma_2 \right) \left(\gamma_2 - 1 \right) \left(c_2 p_1^n + c_1 p_2^n \right) \tau^{n+1}$$

$$\times \left[\varepsilon^{n+1} + p_1^n \tau^{n+1} - c_1 \left(\varepsilon_1^n - \varepsilon_2^n + p_1^n \tau_1^n - p_2^n \tau_2^n \right) \right]$$

$$+ \{ - \left[c_1 \left(\gamma_1 - 1 \right) + c_2 \left(\gamma_2 - 1 \right) \right] \varepsilon^{n+1}$$

$$- \left(\gamma_2 - 1 \right) \left(c_1 p_2^n + c_2 p_1^n \right) \tau^{n+1}$$

$$+ c_2 \left(\gamma_1 - \gamma_2 \right) \left[p_1^n \tau_1^{n+1} - c_1 \left(\varepsilon_1^n - \varepsilon_2^n + p_1^n \tau_1^n - p_2^n \tau_2^n \right) \right] \}^2 \Big]^{1/2} \Big\} \quad (A25)$$

$$\varepsilon_2^{n+1} = \frac{1}{2} \left[c_2 \left(c_1 + c_2 \right) \left(\gamma_1 - \gamma_2 \right) \right]^{-1}$$

$$\times \Big\{ \left(\gamma_1 - 1 \right) \left(c_1 + c_2 \right) \varepsilon^{n+1} + \left[c_2 \left(\gamma_1 - 1 \right) p_1^n + c_1 \left(\gamma_2 - 1 \right) p_2^n \right] \tau^{n+1}$$

$$+ c_2 \left(\gamma_1 - \gamma_2 \right) \left[\varepsilon^{n+1} - c_1 \left(\varepsilon_1^n - \varepsilon_2^n + p_1^n \tau_1^n - p_2^n \tau_2^n \right) \right]$$

$$- \Big[4 c_2 \left(\gamma_1 - \gamma_2 \right) \left(\gamma_2 - 1 \right) \left(c_2 p_1^n + c_1 p_2^n \right) \tau^{n+1}$$

$$\times \left[\varepsilon^{n+1} + p_1^n \tau^{n+1} - c_1 \left(\varepsilon_1^n - \varepsilon_2^n + p_1^n \tau_1^n - p_2^n \tau_2^n \right) \right]$$

$$+ \{ - \left[c_1 \left(\gamma_1 - 1 \right) + c_2 \left(\gamma_2 - 1 \right) \right] \varepsilon^{n+1}$$

$$+ \left(\gamma_2 - 1 \right) \left(c_1 p_2^n + c_2 p_1^n \right) \tau^{n+1}$$

$$- c_2 \left(\gamma_1 - \gamma_2 \right) \left[p_1^n \tau_1^{n+1} + c_1 \left(\varepsilon_1^n - \varepsilon_2^n + p_1^n \tau_1^n - p_2^n \tau_2^n \right) \right] \}^2 \Big]^{1/2} \Big\} \quad (A26)$$

$$\tau_1^{n+1} = \frac{1}{2} \left[c_1 \left(\gamma_1 - \gamma_2 \right) \left(c_1 p_2^n + c_2 p_1^n \right) \right]^{-1}$$

$$\times \Big\{ \left[c_1 \left(\gamma_1 - 1 \right) + c_2 \left(\gamma_2 - 1 \right) \right] \varepsilon^{n+1} + \left(\gamma_1 - 1 \right) \left(c_1 p_2^n + c_2 p_1^n \right) \tau^{n+1}$$

$$+ c_1 \left(\gamma_1 - \gamma_2 \right) \left[p_2^n \tau^{n+1} + c_2 \left(\varepsilon_1^n - \varepsilon_2^n + p_1^n \tau_1^n - p_2^n \tau_2^n \right) \right]$$

$$+ \Big[4 c_2 \left(\gamma_1 - \gamma_2 \right) \left(\gamma_2 - 1 \right) \left(c_2 p_1^n + c_1 p_2^n \right) \tau^{n+1}$$

$$\times \Big[\varepsilon^{n+1} + p_1^n \tau^{n+1} - c_1 \left(\varepsilon_1^n - \varepsilon_2^n + p_1^n \tau_1^n - p_2^n \tau_2^n \right) \Big]$$

$$+ \{ - \left[c_1 \left(\gamma_1 - 1 \right) + c_2 \left(\gamma_2 - 1 \right) \right] \varepsilon^{n+1}$$

$$- \left(\gamma_2 - 1 \right) \left(c_1 p_2^n + c_2 p_1^n \right) \tau^{n+1}$$

$$+ c_2 (\gamma_1 - \gamma_2) \Big[p_1^n \tau_1^{n+1} - c_1 \left(\varepsilon_1^n - \varepsilon_2^n + p_1^n \tau_1^n - p_2^n \tau_2^n \right) \Big] \}^2 \Big]^{1/2} \Big\} \quad (A27)$$

$$\tau_2^{n+1} = -\frac{1}{2} \left[c_2 \left(\gamma_1 - \gamma_2 \right) \left(c_1 p_2^n + c_2 p_1^n \right) \right]^{-1}$$

$$\times \Big\{ \left[c_1 \left(\gamma_1 - 1 \right) + c_2 \left(\gamma_2 - 1 \right) \right] \varepsilon^{n+1} + \left(\gamma_2 - 1 \right) \left(c_1 p_2^n + c_2 p_1^n \right) \tau^{n+1}$$

$$- c_2 \left(\gamma_1 - \gamma_2 \right) \Big[p_1^n \tau^{n+1} - c_1 \left(\varepsilon_1^n - \varepsilon_2^n + p_1^n \tau_1^n - p_2^n \tau_2^n \right) \Big]$$

$$+ \Big[4 c_2 \left(\gamma_1 - \gamma_2 \right) \left(\gamma_2 - 1 \right) \left(c_2 p_1^n + c_1 p_2^n \right) \tau^{n+1}$$

$$\times \Big[\varepsilon^{n+1} + p_1^n \tau^{n+1} - c_1 \left(\varepsilon_1^n - \varepsilon_2^n + p_1^n \tau_1^n - p_2^n \tau_2^n \right) \Big]$$

$$+ \{ - \left[c_1 \left(\gamma_1 - 1 \right) + c_2 \left(\gamma_2 - 1 \right) \right] \varepsilon^{n+1}$$

$$- \left(\gamma_2 - 1 \right) \left(c_1 p_2^n + c_2 p_1^n \right) \tau^{n+1}$$

$$+ c_2 (\gamma_1 - \gamma_2) \Big[p_1^n \tau_1^{n+1} - c_1 \left(\varepsilon_1^n - \varepsilon_2^n + p_1^n \tau_1^n - p_2^n \tau_2^n \right) \Big] \}^2 \Big]^{1/2} \Big\} \quad (A28)$$

A.3.3 Fully explicit, non-identical gases, second solution

When $\gamma_1 \neq \gamma_2$, a second solution is given as:

$$p = \frac{1}{2} \left[\left(c_1 + c_2 \right) \tau^{n+1} \right]^{-1}$$

$$\times \Big\{ \quad \left[c_1 \left(\gamma_1 - 1 \right) + c_2 \left(\gamma_2 - 1 \right) \right] \varepsilon^{n+1}$$

$$+ \left[c_2 \left(\gamma_1 - 1 \right) p_1^n + c_1 \left(\gamma_2 - 1 \right) p_2^n \right] \tau^{n+1}$$

$$+ \; c_1 c_2 \left(\gamma_1 - \gamma_2 \right) \left(\varepsilon_1^n - \varepsilon_2^n + p_1^n \tau_1^n - p_2^n \tau_2^n \right)$$

$$+ \Big[4 c_2 \left(\gamma_1 - \gamma_2 \right) \left(\gamma_2 - 1 \right) \left(c_2 p_1^n + c_1 p_2^n \right) \tau^{n+1}$$

$$\times \Big[\varepsilon^{n+1} + p_1^n \tau^{n+1} - c_1 \left(\varepsilon_1^n - \varepsilon_2^n + p_1^n \tau_1^n - p_2^n \tau_2^n \right) \Big]$$

$$+ \{ - \left[c_1 \left(\gamma_1 - 1 \right) + c_2 \left(\gamma_2 - 1 \right) \right] \varepsilon^{n+1}$$

$$- \left(\gamma_2 - 1 \right) \left[c_2 p_1^n + c_1 p_2^n \right] \tau^{n+1}$$

$$+ c_2 \left(\gamma_1 - \gamma_2 \right) \left[p_1^n \tau_1^n - c_1 \left(\varepsilon_1^n - \varepsilon_2^n + p_1^n \tau_1^n - p_2^n \tau_2^n \right) \right] \}^2 \Big]^{1/2} \Big\} \quad (A29)$$

$$\varepsilon_1^{n+1} = \frac{1}{2}\left[\, c_1\,(c_1+c_2)\,(\gamma_1-\gamma_2)\right]^{-1}$$

$$\times\Big\{-(\gamma_2-1)\,(c_1+c_2)\,\varepsilon^{n+1} - \left[c_2\,(\gamma_1-1)\,p_1^n + c_1\,(\gamma_2-1)\,p_2^n\right]\tau^{n+1}$$

$$+c_1\,(\gamma_1-\gamma_2)\left[\varepsilon^{n+1} + c_2\,(\varepsilon_1^n - \varepsilon_2^n + p_1^n\tau_1^n - p_2^n\tau_2^n)\right]$$

$$+\Big[\,4c_2\,(\gamma_1-\gamma_2)\,(\gamma_2-1)\,(c_2p_1^n + c_1p_2^n)\,\tau^{n+1}$$

$$\times\left[\varepsilon^{n+1} + p_1^n\tau^{n+1} - c_1\,(\varepsilon_1^n - \varepsilon_2^n + p_1^n\tau_1^n - p_2^n\tau_2^n)\right]$$

$$+\{-\left[c_1\,(\gamma_1-1) + c_2\,(\gamma_2-1)\right]\varepsilon^{n+1}$$

$$-(\gamma_2-1)\,(c_1p_2^n + c_2p_1^n)\,\tau^{n+1}$$

$$+c_2(\gamma_1-\gamma_2)\left[p_1^n\tau_1^{n+1} - c_1\,(\varepsilon_1^n - \varepsilon_2^n + p_1^n\tau_1^n - p_2^n\tau_2^n)\right]\}^2\Big]^{1/2}\Big\} \quad (A30)$$

$$\varepsilon_2^{n+1} = \frac{1}{2}\left[\, c_2\,(c_1+c_2)\,(\gamma_1-\gamma_2)\right]^{-1}$$

$$\times\Big\{(\gamma_1-1)\,(c_1+c_2)\,\varepsilon^{n+1} + \left[c_2\,(\gamma_1-1)\,p_1^n + c_1\,(\gamma_2-1)\,p_2^n\right]\tau^{n+1}$$

$$+c_2\,(\gamma_1-\gamma_2)\left[\varepsilon^{n+1} - c_1\,(\varepsilon_1^n - \varepsilon_2^n + p_1^n\tau_1^n - p_2^n\tau_2^n)\right]$$

$$-\Big[\,4c_2\,(\gamma_1-\gamma_2)\,(\gamma_2-1)\,(c_2p_1^n + c_1p_2^n)\,\tau^{n+1}$$

$$\times\left[\varepsilon^{n+1} + p_1^n\tau^{n+1} - c_1\,(\varepsilon_1^n - \varepsilon_2^n + p_1^n\tau_1^n - p_2^n\tau_2^n)\right]$$

$$+\{-\left[c_1\,(\gamma_1-1) + c_2\,(\gamma_2-1)\right]\varepsilon^{n+1}$$

$$-(\gamma_2-1)\,(c_2p_1^n + c_1p_2^n)\,\tau^{n+1}$$

$$+c_2(\gamma_1-\gamma_2)\left[p_1^n\tau_1^{n+1} - c_1\,(\varepsilon_1^n - \varepsilon_2^n + p_1^n\tau_1^n - p_2^n\tau_2^n)\right]\}^2\Big]^{1/2}\Big\} \quad (A31)$$

$$\tau_1^{n+1} = \frac{1}{2}\left[\, c_1\,(\gamma_1-\gamma_2)\,(c_2p_1^n + c_1p_2^n)\right]^{-1}$$

$$\times\Big\{\left[c_1\,(\gamma_1-1) + c_2\,(\gamma_2-1)\right]\varepsilon^{n+1} + (\gamma_1-1)\,(c_2p_1^n + c_1p_2^n)\,\tau^{n+1}$$

$$+c_1\,(\gamma_1-\gamma_2)\left[p_2^n\tau^{n+1} + c_2\,(\varepsilon_1^n - \varepsilon_2^n + p_1^n\tau_1^n - p_2^n\tau_2^n)\right]$$

$$-\Big[\,4c_2\,(\gamma_1-\gamma_2)\,(\gamma_2-1)\,(c_2p_1^n + c_1p_2^n)\,\tau^{n+1}$$

$$\times\left[\varepsilon^{n+1} - p_1^n\tau^{n+1} - c_1\,(\varepsilon_1^n - \varepsilon_2^n + p_1^n\tau_1^n - p_2^n\tau_2^n)\right]$$

$$+\{-\left[c_1\,(\gamma_1-1) + c_2\,(\gamma_2-1)\right]\varepsilon^{n+1}$$

$$-(\gamma_2-1)\,(c_2p_1^n + c_1p_2^n)\,\tau^{n+1}$$

$$+c_2(\gamma_1-\gamma_2)\left[p_1^n\tau_1^{n+1} - c_1\,(\varepsilon_1^n - \varepsilon_2^n + p_1^n\tau_1^n - p_2^n\tau_2^n)\right]\}^2\Big]^{1/2}\Big\} \quad (A32)$$

$$\tau_2^{n+1} = \frac{1}{2}\left[\, c_2\,(\gamma_1-\gamma_2)\,(c_1p_2^n + c_2p_1^n)\right]^{-1}$$

$$\times \left\{ - \left[c_1 \left(\gamma_1 - 1 \right) + c_2 \left(\gamma_2 - 1 \right) \right] \varepsilon^{n+1} - \left(\gamma_2 - 1 \right) \left(c_1 p_2^n + c_2 p_1^n \right) \tau^{n+1} \right.$$

$$+ c_2 \left(\gamma_1 - \gamma_2 \right) \left[p_1^n \tau^{n+1} - c_1 \left(\varepsilon_1^n - \varepsilon_2^n + p_1^n \tau_1^n - p_2^n \tau_2^n \right) \right]$$

$$+ \left[4 c_2 \left(\gamma_1 - \gamma_2 \right) \left(\gamma_2 - 1 \right) \left(c_2 p_1^n + c_1 p_2^n \right) \tau^{n+1} \right.$$

$$\times \left[\varepsilon^{n+1} + p_1^n \tau^{n+1} - c_1 \left(\varepsilon_1^n - \varepsilon_2^n + p_1^n \tau_1^n - p_2^n \tau_2^n \right) \right]$$

$$+ \left\{ - \left[c_1 \left(\gamma_1 - 1 \right) + c_2 \left(\gamma_2 - 1 \right) \right] \varepsilon^{n+1} \right.$$

$$- \left(\gamma_2 - 1 \right) \left(c_1 p_2^n + c_2 p_1^n \right) \tau^{n+1}$$

$$\left. \left. + c_2 (\gamma_1 - \gamma_2) \left[p_1^n \tau_1^{n+1} - c_1 \left(\varepsilon_1^n - \varepsilon_2^n + p_1^n \tau_1^n - p_2^n \tau_2^n \right) \right] \right\}^2 \right]^{1/2} \quad \text{(A33)}$$

A.4 The Thermodynamically Consistent Model

The "*Thermodynamically Consistent*" assigns the pressure in Eq. (46) to be the arithmetic average of the fully explicit and fully implicit values: $P_1 = \frac{1}{2} \left(p_1^n + p_1^{n+1} \right)$, and $P_2 = \frac{1}{2} \left(p_2^n + p_2^{n+1} \right)$. Symbolic manipulation software can be used to obtain closed-form expressions for the solution in this case. One must again distinguish between the case of identical gases (i.e., $\gamma_1 = \gamma_2 \equiv \gamma$) and non-identical gases (i.e., $\gamma_1 \neq \gamma_2$): there are two solutions in the latter case, both of which are more complicated than in the fully explicit case above.

A.4.1 Thermodynamically consistent, identical gases

When $\gamma_1 = \gamma_2 \equiv \gamma$, the solution is given as:

$$p = (\gamma - 1) \, \varepsilon^{n+1} / \tau^{n+1}, \quad \text{(A34)}$$

$$\varepsilon_1^{n+1} = \left(\varepsilon^{n+1} / \tau^{n+1} \right) \left\{ \left[(\gamma + 1)(c_1 + c_2) \varepsilon^{n+1} + (c_2 p_1^n + c_1 p_2^n) \tau^{n+1} \right] \right\}^{-1}$$

$$\times \left\{ \left[(\gamma + 1) \varepsilon^{n+1} + p_2^n \tau^{n+1} \right] \tau^{n+1} \right.$$

$$\left. + c_2 \left[(\gamma - 1)(\tau_1^n - \tau_2^n) \varepsilon^{n+1} + (2\varepsilon_1^n - 2\varepsilon_2^n + p_1^n \tau_1^n - p_2^n \tau_2^n) \tau^{n+1} \right] \right\} \quad \text{(A35)}$$

$$\varepsilon_2^{n+1} = \left(\varepsilon^{n+1} / \tau^{n+1} \right) \left\{ \left[(\gamma + 1)(c_1 + c_2) \varepsilon^{n+1} + (c_2 p_1^n + c_1 p_2^n) \tau^{n+1} \right] \right\}^{-1}$$

$$\times \left\{ \left[(\gamma + 1) \varepsilon^{n+1} + p_1^n \tau^{n+1} \right] \tau^{n+1} \right.$$

$$\left. - c_1 \left[(\gamma - 1)(\tau_1^n - \tau_2^n) \varepsilon^{n+1} + (2\varepsilon_1^n - 2\varepsilon_2^n + p_1^n \tau_1^n - p_2^n \tau_2^n) \tau^{n+1} \right] \right\} \quad \text{(A36)}$$

$$\tau_1^{n+1} = \left[(\gamma + 1)(c_1 + c_2) \varepsilon^{n+1} + (c_2 p_1^n + c_1 p_2^n) \tau^{n+1} \right]^{-1}$$

$$\times \left\{ \left[(\gamma + 1) \varepsilon^{n+1} + p_2^n \tau^{n+1} \right] \tau^{n+1} \right.$$

$$+c_2 \left[(\gamma - 1) (\tau_1^n - \tau_2^n) \, \varepsilon^{n+1} + (2\varepsilon_1^n - 2\varepsilon_2^n + p_1^n \tau_1^n - p_2^n \tau_2^n) \, \tau^{n+1} \right] \} \quad (A37)$$

$$\tau_2^{n+1} = \left[(\gamma + 1) (c_1 + c_2) \, \varepsilon^{n+1} + (c_2 p_1^n + c_1 p_2^n) \, \tau^{n+1} \right]^{-1}$$
$$\times \left\{ \left[(\gamma + 1) \, \varepsilon^{n+1} + p_1^n \tau^{n+1} \right] \tau^{n+1} \right.$$
$$\left. - c_1 \left[(\gamma - 1) (\tau_1^n - \tau_2^n) \, \varepsilon^{n+1} + (2\varepsilon_1^n - 2\varepsilon_2^n + p_1^n \tau_1^n - p_2^n \tau_2^n) \, \tau^{n+1} \right] \right\} \quad (A38)$$

A.4.2 Thermodynamically consistent, non-identical gases, first solution

When $\gamma_1 \neq \gamma_2$, one solution is given as:

$$p = \frac{1}{2} \left\{ c_1 c_2 (\gamma_1 - \gamma_2) (\tau_1^n - \tau_2^n) - [c_1 (\gamma_2 + 1) + c_2 (\gamma_1 + 1)] \, \tau^{n+1} \right\}^{-1}$$
$$\times \left\{ - [c_1 (\gamma_1 - 1) (\gamma_2 + 1) + c_2 (\gamma_1 + 1) (\gamma_2 - 1)] \, \varepsilon^{n+1} \right.$$
$$+ [c_2 (\gamma_1 - 1) p_1^n + c_1 (\gamma_2 - 1) p_2^n] \, \tau^{n+1}$$
$$- c_1 c_2 (\gamma_1 - \gamma_2) (2\varepsilon_1^n - 2\varepsilon_2^n + p_1^n \tau_1^n - p_2^n \tau_2^n)$$
$$+ \Big[4 (\gamma_1 - 1) (\gamma_2 - 1) (c_2 p_1^n + c_1 p_2^n) \, \varepsilon^{n+1}$$
$$\times \{ [c_1 (\gamma_2 + 1) + c_2 (\gamma_1 + 1)] \, \tau^{n+1} - c_1 c_2 (\gamma_1 - \gamma_2) (\tau_1^n - \tau_2^n) \}$$
$$+ \{ [c_1 (\gamma_1 - 1) (\gamma_2 + 1) + c_2 (\gamma_1 + 1) (\gamma_2 - 1)] \, \varepsilon^{n+1}$$
$$- [c_2 (\gamma_1 - 1) p_1^n + c_1 (\gamma_2 - 1) p_2^n] \, \tau^{n_1}$$
$$\left. + c_1 c_2 (\gamma_1 - \gamma_2) (2\varepsilon_1^n - 2\varepsilon_2^n + p_1^n \tau_1^n - p_2^n \tau_2^n) \}^2 \Big]^{1/2} \right\}, \quad (A39)$$

$$\varepsilon_1^{n+1} = \frac{1}{2c_1 (\gamma_1 - \gamma_2)} \left\{ c_1 c_2 (\gamma_1 - \gamma_2) (\tau_1^n - \tau_2^n) \right.$$
$$\left. - [c_1 (\gamma_2 + 1) + c_2 (\gamma_1 + 1)] \, \tau^{n+1} \right\}^{-1}$$
$$\times \left\{ \{ [c_2 (\gamma_1 - 1) p_1^n + c_1 (\gamma_2 - 1) p_2^n] \, \tau^{n+1} \right.$$
$$+ [c_1 (\gamma_2 + 1) + c_2 (\gamma_1 + 1)] (\gamma_2 - 1) \, \varepsilon^{n+1} \} \, \tau^{n+1}$$
$$- c_1 (\gamma_1 - \gamma_2) [2c_2 (\gamma_2 - 1) (\tau_1^n - \tau_2^n) \, \varepsilon^{n+1}$$
$$+ (\gamma_2 + 1) \, \tau^{n+1} \varepsilon^{n+1} + c_2 (2\varepsilon_1^n - 2\varepsilon_2^n + p_1^n \tau_1^n - p_2^n \tau_2^n) \, \tau^{n+1}]$$
$$+ \tau^{n+1} \Big[4 (\gamma_1 - 1) (\gamma_2 - 1) (c_2 p_1^n + c_1 p_2^n) \, \varepsilon^{n+1}$$
$$\times \{ [c_1 (\gamma_2 + 1) + c_2 (\gamma_1 + 1)] \, \tau^{n+1}$$
$$- c_1 c_2 (\gamma_1 - \gamma_2) (\tau_1^n - \tau_2^n) \}$$
$$+ \{ \ [c_1 (\gamma_1 - 1) (\gamma_2 + 1) + c_2 (\gamma_1 + 1) (\gamma_2 - 1)] \, \varepsilon^{n+1}$$
$$+ [c_2 (\gamma_1 - 1) p_1^n + c_1 (\gamma_2 - 1) p_2^n] \, \tau^{n+1}$$

$$+\, c_1 c_2 \left(\gamma_1 - \gamma_2\right) \left(2\varepsilon_1^n - 2\varepsilon_2^n + p_1^n \tau_1^n - p_2^n \tau_2^n\right)\big\}^2\Big]^{1/2}\Big\} \quad (A40)$$

$$\varepsilon_2^{n+1} = -\frac{1}{2c_2\left(\gamma_1 - \gamma_2\right)} \big\{ c_1 c_2 \left(\gamma_1 - \gamma_2\right) \left(\tau_1^n - \tau_2^n\right)$$
$$- \left[c_1 \left(\gamma_2 + 1\right) + c_2 \left(\gamma_1 + 1\right)\right] \tau^{n+1} \big\}^{-1}$$
$$\times \Big\{ \big\{ \left[c_2 \left(\gamma_1 - 1\right) p_1^n + c_1 \left(\gamma_2 - 1\right) p_2^n\right] \tau^{n+1}$$
$$+ \left[c_1 \left(\gamma_2 + 1\right) + c_2 \left(\gamma_1 + 1\right)\right] \left(\gamma_1 - 1\right) \varepsilon^{n+1} \big\} \tau^{n+1}$$
$$- c_2 \left(\gamma_1 - \gamma_2\right) \big[\, 2c_1 \left(\gamma_1 - 1\right) \left(\tau_1^n - \tau_2^n\right) \varepsilon^{n+1}$$
$$- \left(\gamma_1 + 1\right) \tau^{n+1} \varepsilon^{n+1} + c_1 \left(2\varepsilon_1^n - 2\varepsilon_2^n + p_1^n \tau_1^n - p_2^n \tau_2^n\right) \tau^{n+1}\,\big]$$
$$+ \tau^{n+1} \Big[\, 4 \left(\gamma_1 - 1\right) \left(\gamma_2 - 1\right) \left(c_2 p_1^n + c_1 p_2^n\right) \varepsilon^{n+1}$$
$$\times \big\{ \left[\, c_1 \left(\gamma_2 + 1\right) + c_2 \left(\gamma_1 + 1\right)\right] \tau^{n+1}$$
$$- c_1 c_2 \left(\gamma_1 - \gamma_2\right) \left(\tau_1^n - \tau_2^n\right) \big\}$$
$$+ \big\{ \left[\, c_1 \left(\gamma_1 - 1\right) \left(\gamma_2 + 1\right) + c_2 \left(\gamma_1 + 1\right) \left(\gamma_2 - 1\right)\right] \varepsilon^{n+1}$$
$$- \left[\, c_2 \left(\gamma_1 - 1\right) p_1^n + c_1 \left(\gamma_2 - 1\right) p_2^n\right] \tau^{n+1}$$
$$+ c_1 c_2 \left(\gamma_1 - \gamma_2\right) \left(2\varepsilon_1^n - 2\varepsilon_2^n + p_1^n \tau_1^n - p_2^n \tau_2^n\right)\big\}^2\Big]^{1/2}\Big\}, (A41)$$

$$\tau_1^{n+1} = \frac{1}{2c_1\left(\gamma_1 - \gamma_2\right)} \left(c_2 p_1^n + c_1 p_2^n\right)^{-1}$$
$$\times \Big\{ \left(\gamma_1 - 1\right) \left(c_1 p_2^n + c_2 p_1^n\right) \tau^{n+1}$$
$$+ \left[c_1 \left(\gamma_1 - 1\right) \left(\gamma_2 + 1\right) + c_2 \left(\gamma_1 + 1\right) \left(\gamma_2 - 1\right)\right] \varepsilon^{n+1}$$
$$+ c_1 \left(\gamma_1 - \gamma_2\right) \left[\, p_2^n \tau^{n+1} + c_2 \left(2\varepsilon_1^n - 2\varepsilon_2^n + p_1^n \tau_1^n - p_2^n \tau_2^n\right)\right]$$
$$+ \Big[4 \left(\gamma_1 - 1\right) \left(\gamma_2 - 1\right) \left(c_2 p_1^n + c_1 p_2^n\right) \varepsilon^{n+1}$$
$$\times \big\{ \left[c_1 \left(\gamma_2 + 1\right) + c_2 \left(\gamma_1 + 1\right)\right] \tau^{n+1}$$
$$- c_1 c_2 \left(\gamma_1 - \gamma_2\right) \left(\tau_1^n - \tau_2^n\right) \big\}$$
$$+ \big\{ \left[\, c_1 \left(\gamma_1 - 1\right) \left(\gamma_2 + 1\right) + c_2 \left(\gamma_1 + 1\right) \left(\gamma_2 - 1\right)\right] \varepsilon^{n+1}$$
$$- \left[\, c_2 \left(\gamma_1 - 1\right) p_1^n + c_1 \left(\gamma_2 - 1\right) p_2^n\right] \tau^{n+1}$$
$$+ c_1 c_2 \left(\gamma_1 - \gamma_2\right) \left(2\varepsilon_1^n - 2\varepsilon_2^n + p_1^n \tau_1^n - p_2^n \tau_2^n\right)\big\}^2\Big]^{1/2}\Big\}, \quad (A42)$$

$$\tau_2^{n+1} = -\frac{1}{2c_2\left(\gamma_1 - \gamma_2\right)} \left(c_2 p_1^n + c_1 p_2^n\right)^{-1}$$
$$\times \Big\{ \left(\gamma_2 - 1\right) \left(c_1 p_2^n + c_2 p_1^n\right) \tau^{n+1}$$
$$+ \left[c_1 \left(\gamma_1 - 1\right) \left(1 + \gamma_2\right) + c_2 \left(\gamma_1 + 1\right) \left(\gamma_2 - 1\right)\right] \varepsilon^{n+1}$$

$$-c_2\left(\gamma_1-\gamma_2\right)\left[p_1^n\tau^{n+1}-c_1\left(2\varepsilon_1^n-2\varepsilon_2^n+p_1^n\tau_1^n-p_2^n\tau_2^n\right)\right]$$

$$+\left[4\left(\gamma_1-1\right)\left(\gamma_2-1\right)\left(c_2p_1^n+c_1p_2^n\right)\varepsilon^{n+1}\right.$$

$$\times\left\{\left[c_1\left(\gamma_2+1\right)+c_2\left(\gamma_1+1\right)\right]\tau^{n+1}\right.$$

$$\left.-c_1c_2\left(\gamma_1-\gamma_2\right)\left(\tau_1^n-\tau_2^n\right)\right\}$$

$$+\left\{\left[c_1\left(\gamma_1-1\right)\left(\gamma_2+1\right)+c_2\left(\gamma_1+1\right)\left(\gamma_2-1\right)\right]\varepsilon^{n+1}\right.$$

$$-\left[c_2\left(\gamma_1-1\right)p_1^n+c_1\left(\gamma_2-1\right)p_2^n\right]\tau^{n+1}$$

$$\left.\left.+c_1c_2\left(\gamma_1-\gamma_2\right)\left(2\varepsilon_1^n-2\varepsilon_2^n+p_1^n\tau_1^n-p_2^n\tau_2^n\right)\right\}^2\right]^{1/2}\right\}. \qquad \text{(A43)}$$

A.4.3 Thermodynamically consistent, non-identical gases, second solution

When $\gamma_1\neq\gamma_2$, the second solution is given as:

$$p=-\frac{1}{2}\left\{c_1c_2\left(\gamma_1-\gamma_2\right)\left(\tau_1^n-\tau_2^n\right)-\left[c_1\left(\gamma_2+1\right)+c_2\left(\gamma_1+1\right)\right]\tau^{n+1}\right\}^{-1}$$

$$\times\left\{\;\left[c_1\left(\gamma_1-1\right)\left(\gamma_2+1\right)+c_2\left(\gamma_1+1\right)\left(\gamma_2-1\right)\right]\varepsilon^{n+1}\right.$$

$$-\left[c_2\left(\gamma_1-1\right)p_1^n+c_1\left(\gamma_2-1\right)p_2^n\right]\tau^{n+1}$$

$$+c_1c_2\left(\gamma_1-\gamma_2\right)\left(2\varepsilon_1^n-2\varepsilon_2^n+p_1^n\tau_1^n-p_2^n\tau_2^n\right)$$

$$+\left[4\left(\gamma_1-1\right)\left(\gamma_2-1\right)\left(c_2p_1^n+c_1p_2^n\right)\varepsilon^{n+1}\right.$$

$$\times\left\{\left[c_1\left(\gamma_2+1\right)+c_2\left(\gamma_1+1\right)\right]\tau^{n+1}-c_1c_2\left(\gamma_1-\gamma_2\right)\left(\tau_1^n-\tau_2^n\right)\right\}$$

$$+\left\{\left[c_1\left(\gamma_1-1\right)\left(\gamma_2+1\right)+c_2\left(\gamma_1+1\right)\left(\gamma_2-1\right)\right]\varepsilon^{n+1}\right.$$

$$-\left[c_2\left(\gamma_1-1\right)p_1^n+c_1\left(\gamma_2-1\right)p_2^n\right]\tau^{n_1}$$

$$\left.\left.\left.+c_1c_2\left(\gamma_1-\gamma_2\right)\left(2\varepsilon_1^n-2\varepsilon_2^n+p_1^n\tau_1^n-p_2^n\tau_2^n\right)\right\}^2\right]^{1/2}\right\}, \qquad \text{(A44)}$$

$$\varepsilon_1^{n+1}=\frac{1}{2c_1\left(\gamma_1-\gamma_2\right)}\left\{c_1c_2\left(\gamma_1-\gamma_2\right)\left(\tau_1^n-\tau_2^n\right)\right.$$

$$\left.-\left[c_1\left(\gamma_2+1\right)+c_2\left(\gamma_1+1\right)\right]\tau^{n+1}\right\}^{-1}$$

$$\times\left\{\left\{\left[c_2\left(\gamma_1-1\right)p_1^n+c_1\left(\gamma_2-1\right)p_2^n\right]\tau^{n+1}\right.\right.$$

$$\left.+\left[c_1\left(\gamma_2+1\right)+c_2\left(\gamma_1+1\right)\right]\left(\gamma_2-1\right)\varepsilon^{n+1}\right\}\tau^{n+1}$$

$$-c_1\left(\gamma_1-\gamma_2\right)\left[2c_2\left(\gamma_2-1\right)\left(\tau_1^n-\tau_2^n\right)\varepsilon^{n+1}\right.$$

$$\left.+\left(\gamma_2+1\right)\tau^{n+1}\varepsilon^{n+1}+c_2\left(2\varepsilon_1^n-2\varepsilon_2^n+p_1^n\tau_1^n-p_2^n\tau_2^n\right)\tau^{n+1}\right]$$

$$-\tau^{n+1}\left[4\left(\gamma_1-1\right)\left(\gamma_2-1\right)\left(c_2p_1^n+c_1p_2^n\right)\varepsilon^{n+1}\right.$$

$$\times\left\{\left[c_1\left(\gamma_2+1\right)+c_2\left(\gamma_1+1\right)\right]\tau^{n+1}\right.$$

$$-c_1 c_2 \left(\gamma_1 - \gamma_2\right) \left(\tau_1^n - \tau_2^n\right)\}$$
$$+\{\left[\,c_1 \left(\gamma_1 - 1\right)\left(\gamma_2 + 1\right) + c_2 \left(\gamma_1 + 1\right)\left(\gamma_2 - 1\right)\right] \varepsilon^{n+1}$$
$$-\left[\,c_2 \left(\gamma_1 - 1\right) p_1^n + c_1 \left(\gamma_2 - 1\right) p_2^n\right] \tau^{n+1}$$
$$+ c_1 c_2 \left(\gamma_1 - \gamma_2\right)\left(2\varepsilon_1^n - 2\varepsilon_2^n + p_1^n \tau_1^n - p_2^n \tau_2^n\right)\}^2\big]^{1/2}\Big\} , \quad \text{(A45)}$$

$$\varepsilon_2^{n+1} = -\frac{1}{2c_2 \left(\gamma_1 - \gamma_2\right)} \{c_1 c_2 \left(\gamma_1 - \gamma_2\right) \left(\tau_1^n - \tau_2^n\right)$$
$$- \left[c_1 \left(\gamma_2 + 1\right) + c_2 \left(\gamma_1 + 1\right)\right] \tau^{n+1}\}^{-1}$$
$$\times \Big\{ \{\left[c_2 \left(\gamma_1 - 1\right) p_1^n + c_1 \left(\gamma_2 - 1\right) p_2^n\right] \tau^{n+1}$$
$$+ \left[c_1 \left(\gamma_2 + 1\right) + c_2 \left(\gamma_1 + 1\right)\right]\left(\gamma_1 - 1\right) \varepsilon^{n+1}\} \tau^{n+1}$$
$$- c_2 \left(\gamma_1 - \gamma_2\right)\left[\,2c_1 \left(\gamma_1 - 1\right)\left(\tau_1^n - \tau_2^n\right) \varepsilon^{n+1}\right.$$
$$\left. - \left(\gamma_1 + 1\right) \tau^{n+1}\varepsilon^{n+1} + c_1 \left(2\varepsilon_1^n - 2\varepsilon_2^n + p_1^n \tau_1^n - p_2^n \tau_2^n\right) \tau^{n+1}\right]$$
$$- \tau^{n+1}\big[4 \left(\gamma_1 - 1\right)\left(\gamma_2 - 1\right)\left(c_2 p_1^n + c_1 p_2^n\right) \varepsilon^{n+1}$$
$$\times \{\left[c_1 \left(\gamma_2 + 1\right) + c_2 \left(\gamma_1 + 1\right)\right] \tau^{n+1}$$
$$- c_1 c_2 \left(\gamma_1 - \gamma_2\right) \left(\tau_1^n - \tau_2^n\right)\}$$
$$+\{\left[\,c_1 \left(\gamma_1 - 1\right)\left(\gamma_2 + 1\right) + c_2 \left(\gamma_1 + 1\right)\left(\gamma_2 - 1\right)\right] \varepsilon^{n+1}$$
$$-\left[\,c_2 \left(\gamma_1 - 1\right) p_1^n + c_1 \left(\gamma_2 - 1\right) p_2^n\right] \tau^{n+1}$$
$$+ c_1 c_2 \left(\gamma_1 - \gamma_2\right)\left(2\varepsilon_1^n - 2\varepsilon_2^n + p_1^n \tau_1^n - p_2^n \tau_2^n\right)\}^2\big]^{1/2}\Big\} , \quad \text{(A46)}$$

$$\tau_1^{n+1} = \frac{1}{2c_1 \left(\gamma_1 - \gamma_2\right)} \left(c_2 p_1^n + c_1 p_2^n\right)^{-1}$$
$$\times \Big\{\left(\gamma_1 - 1\right)\left(c_2 p_1^n + c_1 p_2^n\right) \tau^{n+1}$$
$$+ \left[c_1 \left(\gamma_1 - 1\right)\left(\gamma_2 + 1\right) + c_2 \left(\gamma_1 + 1\right)\left(\gamma_2 - 1\right)\right] \varepsilon^{n+1}$$
$$+ c_1 \left(\gamma_1 - \gamma_2\right)\left[\,p_2^n \tau^{n+1} + c_2 \left(2\varepsilon_1^n - 2\varepsilon_2^n + p_1^n \tau_1^n - p_2^n \tau_2^n\right)\right]$$
$$- \big[4 \left(\gamma_1 - 1\right)\left(\gamma_2 - 1\right)\left(c_2 p_1^n + c_1 p_2^n\right) \varepsilon^{n+1}$$
$$\times \{\left[c_1 \left(\gamma_2 + 1\right) + c_2 \left(\gamma_1 + 1\right)\right] \tau^{n+1}$$
$$- c_1 c_2 \left(\gamma_1 - \gamma_2\right) \left(\tau_1^n - \tau_2^n\right)\}$$
$$+\{\left[c_1 \left(\gamma_1 - 1\right)\left(\gamma_2 + 1\right) + c_2 \left(\gamma_1 + 1\right)\left(\gamma_2 - 1\right)\right] \varepsilon^{n+1}$$
$$- \tau^{n+1}\left[c_2 \left(\gamma_1 - 1\right) p_1^n + c_1 \left(\gamma_2 - 1\right) p_2^n\right]$$
$$+ c_1 c_2 \left(\gamma_1 - \gamma_2\right)\left(2\varepsilon_1^n - 2\varepsilon_2^n + p_1^n \tau_1^n - p_2^n \tau_2^n\right)\}^2\big]^{1/2}\Big\} , \quad \text{(A47)}$$

$$\tau_2^{n+1} = -\frac{1}{2c_2 \left(\gamma_1 - \gamma_2\right)} \left(c_2 p_1^n + c_1 p_2^n\right)^{-1}$$

$$\times \Big\{ (\gamma_2 - 1)\,(c_2 p_1^n + c_1 p_2^n)\,\tau^{n+1}$$
$$+\left[c_1\,(\gamma_1 - 1)\,(\gamma_2 + 1) + c_2\,(\gamma_1 + 1)\,(\gamma_2 - 1) \right] \varepsilon^{n+1}$$
$$-c_2\,(\gamma_1 - \gamma_2)\left[p_1^n \tau^{n+1} - c_1\,(2\varepsilon_1^n - 2\varepsilon_2^n + p_1^n \tau_1^n - p_2^n \tau_2^n) \right]$$
$$-\Big[4\,(\gamma_1 - 1)\,(\gamma_2 - 1)\,(c_2 p_1^n + c_1 p_2^n)\,\varepsilon^{n+1}$$
$$\times \{ \left[c_1\,(\gamma_2 + 1) + c_2\,(\gamma_1 + 1) \right] \tau^{n+1}$$
$$-c_1 c_2\,(\gamma_1 - \gamma_2)\,(\tau_1^n - \tau_2^n) \}$$
$$+\{ \left[c_1\,(\gamma_1 - 1)\,(\gamma_2 + 1) + c_2\,(\gamma_1 + 1)\,(\gamma_2 - 1) \right] \varepsilon^{n+1}$$
$$- \left[c_2\,(\gamma_1 - 1)\,p_1^n + c_1\,(\gamma_2 - 1)\,p_2^n \right] \tau^{n+1}$$
$$+c_1 c_2\,(\gamma_1 - \gamma_2)\,(2\varepsilon_1^n - 2\varepsilon_2^n + p_1^n \tau_1^n - p_2^n \tau_2^n) \}^2 \Big]^{1/2} \Big\}. \qquad \text{(A48)}$$

Appendix B: Jacobian Elements for the Instantaneous Equilibration, Polytropic Gas Model

In this appendix we provide explicit formulae for the elements of the Jacobian matrix used in the Newton iteration for the solution of Eqs. (50)–(53) describing the instantaneous pressure equilibration model. The elements of this matrix depend on the modeling choice made in describing the pressure term P_k in Eq. (53).

The first two rows of the Jacobian are independent of the EOS. The elements of these two rows are given by:

$$\frac{\partial f_1}{\partial x_1} = c_1 \,, \quad \frac{\partial f_1}{\partial x_2} = 0 \,, \quad \frac{\partial f_1}{\partial x_3} = c_2 \,, \quad \frac{\partial f_1}{\partial x_4} = 0 \,, \tag{B1}$$

$$\frac{\partial f_2}{\partial x_1} = 0 \,, \quad \frac{\partial f_2}{\partial x_2} = c_1 \,, \quad \frac{\partial f_2}{\partial x_3} = 0 \,, \quad \frac{\partial f_2}{\partial x_4} = c_2 \,, \tag{B2}$$

The fourth row of the Jacobian, while independent of the closure model, depends on the EOS through the pressure term:

$$\frac{\partial f_4}{\partial x_1} = \frac{\partial \mathcal{P}_1}{\partial x_1} = \frac{\partial \mathcal{P}_1}{\partial \tau_1} \,, \tag{B3}$$

$$\frac{\partial f_4}{\partial x_2} = \frac{\partial \mathcal{P}_1}{\partial x_2} = \frac{\partial \mathcal{P}_1}{\partial \varepsilon_1} \,, \tag{B4}$$

$$\frac{\partial f_4}{\partial x_3} = -\frac{\partial \mathcal{P}_2}{\partial x_3} = -\frac{\partial \mathcal{P}_2}{\partial \tau_2} \,, \tag{B5}$$

$$\frac{\partial f_4}{\partial x_4} = -\frac{\partial \mathcal{P}_2}{\partial x_4} = -\frac{\partial \mathcal{P}_2}{\partial \varepsilon_2} \,. \tag{B6}$$

For the (incomplete) polytropic EOS,

$$\mathcal{P}(\tau, \varepsilon) \equiv (\gamma - 1)\, \varepsilon\, \tau^{-1} \,, \tag{B7}$$

these terms can be evaluated explicitly:

$$\frac{\partial f_4}{\partial x_1} = -(\gamma_1 - 1)\, x_2\, x_1^{-2} = -(\gamma_1 - 1)\, \varepsilon_1\, \tau_1^{-2} \,, \tag{B8}$$

$$\frac{\partial f_4}{\partial x_2} = \ (\gamma_1 - 1)\, x_1^{-1} \ = \ (\gamma_1 - 1)\, \tau_1^{-1} \,, \tag{B9}$$

$$\frac{\partial f_4}{\partial x_3} = \ (\gamma_2 - 1)\, x_4\, x_3^{-2} = \ (\gamma_2 - 1)\, \varepsilon_2\, \tau_2^{-2} \,, \tag{B10}$$

$$\frac{\partial f_4}{\partial x_4} = -(\gamma_2 - 1)\, x_3^{-1} \ = -(\gamma_2 - 1)\, \tau_2^{-1} \,. \tag{B11}$$

The third row of the Jacobian depends on both the closure model and the EOS through the pressure term. The modeling choice of when the pressure is evaluated affects the specific form assumed by the Jacobian element in this row.

B.2 The Fully Implicit Model

In the *"Fully Implicit"* case, $P_1 = p_1^{n+1} = \mathcal{P}_1(\tau_1^{n+1}, \varepsilon_1^{n+1})$ and $P_2 = p_2^{n+1} = \mathcal{P}_2(\tau_2^{n+1}, \varepsilon_2^{n+1})$, so that

$$
\begin{aligned}
f_3 &\equiv \varepsilon_1^{n+1} - \varepsilon_1^n + \mathcal{P}_1(\tau_1^{n+1}, \varepsilon_1^{n+1})(\tau_1^{n+1} - \tau_1^n) \\
&\quad - \left[\varepsilon_2^{n+1} - \varepsilon_2^n + \mathcal{P}_2(\tau_2^{n+1}, \varepsilon_2^{n+1})(\tau_2^{n+1} - \tau_2^n) \right]
\end{aligned}
\tag{B12}
$$

$$
\Rightarrow \quad
\begin{aligned}
f_3 &\equiv x_2 - \varepsilon_1^n + \mathcal{P}_1(x_1, x_2)(x_1 - \tau_1^n) \\
&\quad - \left[x_4 - \varepsilon_2^n + \mathcal{P}_2(x_3, x_4)(x_3 - \tau_2^n) \right] .
\end{aligned}
\tag{B13}
$$

The corresponding Jacobian elements are:

$$
\begin{aligned}
\frac{\partial f_3}{\partial x_1} &= \frac{\partial \mathcal{P}_1}{\partial x_1} (x_1 - \tau_1^n) + \mathcal{P}_1(x_1, x_2) \\
&= \frac{\partial f_4}{\partial x_1} (x_1 - \tau_1^n) + \mathcal{P}_1(x_1, x_2),
\end{aligned}
\tag{B14}
$$

$$
\begin{aligned}
\frac{\partial f_3}{\partial x_2} &= 1 + \frac{\partial \mathcal{P}_1}{\partial x_2} (x_1 - \tau_1^n) \\
&= 1 + \frac{\partial f_4}{\partial x_2} (x_1 - \tau_1^n) ,
\end{aligned}
\tag{B15}
$$

$$
\begin{aligned}
\frac{\partial f_3}{\partial x_3} &= -\frac{\partial \mathcal{P}_2}{\partial x_3} (x_3 - \tau_2^n) - \mathcal{P}_2(x_3, x_4) \\
&= \frac{\partial f_4}{\partial x_3} (x_3 - \tau_2^n) - \mathcal{P}_2(x_3, x_4),
\end{aligned}
\tag{B16}
$$

$$
\begin{aligned}
\frac{\partial f_3}{\partial x_4} &= -1 - \frac{\partial \mathcal{P}_2}{\partial x_4} (x_3 - \tau_2^n) \\
&= -1 + \frac{\partial f_4}{\partial x_4} (x_3 - \tau_2^n) .
\end{aligned}
\tag{B17}
$$

B.3 The Fully Explicit Model

For the "*Fully Explicit*" case, $P_1 = p_1^n$ and $P_2 = p_2^n$, independent of the updated state vector $\mathbf{x}$, so that

$$
\begin{aligned}
f_3 &\equiv \varepsilon_1^{n+1} - \varepsilon_1^n + p_1^n(\tau_1^{n+1} - \tau_1^n) \\
&\quad - \left[\varepsilon_2^{n+1} - \varepsilon_2^n + p_2^n(\tau_2^{n+1} - \tau_2^n) \right] ,
\end{aligned}
\tag{B18}
$$

$$
\begin{aligned}
\Rightarrow \quad f_3 &\equiv x_2 - \varepsilon_1^n + p_1^n(x_1 - \tau_1^n) \\
&\quad - \left[x_4 - \varepsilon_2^n + p_2^n(x_3 - \tau_2^n) \right] .
\end{aligned}
\tag{B19}
$$

The corresponding Jacobian elements are:

$$
\frac{\partial f_3}{\partial x_1} = p_1^n ,
\tag{B20}
$$

$$
\frac{\partial f_3}{\partial x_2} = 1 ,
\tag{B21}
$$

$$
\frac{\partial f_3}{\partial x_3} = -p_2^n ,
\tag{B22}
$$

$$
\frac{\partial f_3}{\partial x_4} = -1 .
\tag{B23}
$$

B.3 The Thermodynamically Consistent Model

For the "*Thermodynamically Consistent*" model, $P_1 = \frac{1}{2}\left(p_1^n + p_1^{n+1}\right)$ and $P_2 = \frac{1}{2}\left(p_2^n + p_2^{n+1}\right)$, which imply

$$
\begin{aligned}
f_3 &\equiv \varepsilon_1^{n+1} - \varepsilon_1^n + \frac{1}{2}\left(p_1^n + \mathcal{P}_1(\tau_1^{n+1}, \varepsilon_1^{n+1})\right)(\tau_1^{n+1} - \tau_1^n) \\
&\quad - \left[\varepsilon_2^{n+1} - \varepsilon_2^n + \frac{1}{2}\left(p_2^n + \mathcal{P}_2(\tau_2^{n+1}, \varepsilon_2^{n+1})\right)(\tau_2^{n+1} - \tau_2^n) \right] ,
\end{aligned}
\tag{B24}
$$

$$
\begin{aligned}
\Rightarrow \quad f_3 &\equiv x_2 - \varepsilon_1^n + \frac{1}{2}\left(p_1^n + \mathcal{P}_1(x_1, x_2)\right)(x_1 - \tau_1^n) \\
&\quad - \left[x_4 - \varepsilon_2^n + \frac{1}{2}\left(p_2^n + \mathcal{P}_2(x_3, x_4)\right)(x_3 - \tau_2^n) \right] .
\end{aligned}
\tag{B25}
$$

The corresponding Jacobian elements are:

$$
\frac{\partial f_3}{\partial x_1} = \frac{1}{2}\frac{\partial \mathcal{P}_1}{\partial x_1}(x_1 - \tau_1^n) + \frac{1}{2}\left(p_1^n + \mathcal{P}_1(x_1, x_2)\right)
$$

$$= \quad \frac{1}{2}\frac{\partial f_4}{\partial x_1}\ (x_1 - \tau_1^n) + \frac{1}{2}\ (p_1^n + \mathcal{P}_1(x_1, x_2))\ , \tag{B26}$$

$$\frac{\partial f_3}{\partial x_2} = \quad 1 + \frac{1}{2}\frac{\partial \mathcal{P}_1}{\partial x_2}\ (x_1 - \tau_1^n)$$

$$= \quad 1 + \frac{1}{2}\frac{\partial f_4}{\partial x_2}\ (x_1 - \tau_1^n)\ , \tag{B27}$$

$$\frac{\partial f_3}{\partial x_3} = -\frac{1}{2}\frac{\partial \mathcal{P}_2}{\partial x_3}\ (x_3 - \tau_2^n) - \frac{1}{2}\ (p_2^n + \mathcal{P}_2(x_3, x_4))$$

$$= \quad \frac{1}{2}\frac{\partial f_4}{\partial x_3}\ (x_3 - \tau_2^n) - \frac{1}{2}\ (p_2^n + \mathcal{P}_2(x_3, x_4))\ , \tag{B28}$$

$$\frac{\partial f_3}{\partial x_4} = -1 - \frac{1}{2}\frac{\partial \mathcal{P}_2}{\partial x_4}\ (x_3 - \tau_2^n)$$

$$= -1 + \frac{1}{2}\frac{\partial f_4}{\partial x_4}\ (x_3 - \tau_2^n)\ , \tag{B29}$$

References

[1] N. Andrianov. *Analytical and numerical investigation of two-phase flows*. PhD thesis, Universität Magdeburg, 2003.

[2] M. Arora and P.L. Roe. On postshock oscillations due to shock capturing schemes in unsteady flows. *J. Comput. Phys.*, 130:25–40, 1997.

[3] J.W. Banks, D.W Schwendeman, A.K. Kapila, and W.D. Henshaw. A high-resolution Godunov method for compressible multi-material flow on overlapping grids. *J. Comput. Phys.*, 223:262–297, 2007.

[4] A. Barlow. A new Lagrangian scheme for multimaterial cells. In *Proceedings of European Congress on Computational Methods in Applied Sciences and Engineering*, pages 235–294. ECCOMAS Computational Fluid Dynamics Conference, 2001.

[5] A.L. Bauer, D.E. Burton, E.J. Caramana, R. Loubere, M.J. Shashkov, and P.P. Whalen. The internal consistency, stability, and accuracy of the discrete, compatible formulation of Lagrangian hydrodynamics. *J. Comput. Phys.*, 218:572–593, 2006.

[6] J. Campbell and M. Shashkov. A tensor artificial viscosity using a mimetic finite difference algorithm. *J. Comput. Phys.*, 172:739–765, 2001.

[7] E.J. Caramana, D.E. Burton, M.J. Shashkov, and P.P. Whalen. The construction of compatible hydrodynamics algorithms utilizing conservation of total energy. *J. Comput. Phys.*, 146:227–262, 1999.

[8] P. Colella and H.M Glaz. Efficient solution algorithm for the Riemann problem for real gases. *J. Comput. Phys.*, 59:264–289, 1985.

[9] V.I. Delov and V.V. Sadchikov. Comparison of several models for computation of thermodynamical parameters for heterogeneous lagrangian cells. *VANT (Mathematical Modeling of Physical Processes)*, 1:57–70, 2005.

[10] B. Després and F. Lagoutière. Numerical resolution of a two-component compressible fluid model with interfaces. *Prog. Comput. Fluid Dyn.*, 7:295–310, 2007.

[11] E.A. Goncharov and Yu. Yanilkin. New method for computations of thermodynamical states of the materials in the mixed cells. *VANT (Mathematical Modeling of Physical Processes)*, 3:16–30, 2004.

[12] J.J. Gottlieb and C.P.T. Groth. Assessment of Riemann solvers for unsteady one-dimensional inviscid flows of perfect gases. *J. Comput. Phys.*, 78:437–458, 1988.

[13] O.A. Hurricane and P.L. Miller. Shock transmission and reflection from a material interface and subsequent reflection from a hard boundary. Technical Report UCRL-ID-132586, Lawrence Livermore National Laboratory, 1998.

[14] E. Johnson and T. Colonius. Implementation of WENO schemes in compressible multicomponent flow problems. *J. Comput. Phys.*, 219:715–732, 2006.

[15] F. Lagoutière. *Modélisation Mathématique et Résolution Numérique de Problèmes de Fluides Compressibles à Plusieurs Constituants*. PhD thesis, Université Pierre-et-Marie-Curie, Paris VI, 2000.

[16] R. Landshoff. A numerical method for treating fluid flow in the presence of shocks. Technical Report LA-1930, Los Alamos Scientific Laboratory, 1955.

[17] R. LeVeque. *Finite Volume Methods for Hyperbolic Problems*. Cambridge University Press, Cambridge, UK, 2002.

[18] R. Liska and B. Wendroff. Comparison of several difference schemes on 1D and 2D test problems for the Euler equations. *SIAM J. Sci. Comput.*, 25:995–1017, 2003.

[19] R. Loubère, M. Shashkov, B. Després, and F. Lagoutière. A Mixing Model for Multimaterial Computations in Fluid Dynamics. Technical Report LA-UR-04-6694, Los Alamos National Laboratory, 2004.

[20] H. Luo, J. Baum, and R. Löhner. On the computation of multi-material flows using ALE formation. *J. Comput. Phys.*, 194:304–328, 2004.

[21] B. Plohr. Shockless acceleration of thin plates modeled by a tracked random choice method. *AIAA J.*, 26:470–478, 1988.

[22] L. Quartapelle, L. Castelletti, A. Guardone, and G. Quaranta. Solution of the Riemann problem of classical gasdynamics. *J. Comput. Phys.*, 190:118–140, 2003.

[23] R. Saurel and R. Abgrall. A multiphase Godunov method for compressible multifluid and multiphase flows. *J. Comput. Phys.*, 150:425–467, 1999.

[24] M. Shashkov. Closure models for multimaterial cells in arbitrary Lagrangian-Eulerian hydrocodes. *Int. J. Numer. Meth. Fluids*, 56:1497–1504, 2007.

[25] G. Sod. A survey of several finite difference methods for systems of nonlinear hyperbolic conservation laws. *J. Comput. Phys.*, 27:1–31, 1978.

[26] R.E. Tipton. Cale mixed zone pressure relaxation model. Unpublished notes, 1989.

[27] E. Toro. *Riemann Solvers and Numerical Methods for Fluid Dynamics: A Practical Introduction.* Springer, Heidelberg, 1999.

[28] J. von Neumann and R. Richtmyer. A method for the numerical calculation of hydrodynamic shocks. *J. Appl. Phys.*, 21:232–237, 1950.

	100	200	400	800	$\mathcal{A}$	σ
ρ	8.56×10^{-3}	4.30×10^{-3}	2.16×10^{-3}	1.09×10^{-3}	0.83	0.99
p	8.62×10^{-3}	4.32×10^{-3}	2.19×10^{-3}	1.09×10^{-3}	0.83	0.99
e	2.48×10^{-2}	1.27×10^{-2}	6.21×10^{-3}	3.12×10^{-3}	2.52	1.00
u	2.30×10^{-2}	1.16×10^{-2}	5.32×10^{-3}	2.71×10^{-3}	2.75	1.04

Table 1: L_1 norms of the difference between exact and computed Sod problem results, computed pointwise at $t = 0.2$, for the given variables with the indicated number of points on the unit interval. The prefactor $\mathcal{A}$ and convergence rate σ are least-squares fits to the relation given in Eq. (82). The values of σ close to unity suggest first-order convergence.

	100	200	400	800	$\mathcal{A}$	σ
ρ	1.07×10^{-2}	5.22×10^{-3}	2.61×10^{-3}	1.35×10^{-3}	1.04	1.00
p	1.70×10^{-2}	8.23×10^{-3}	4.12×10^{-3}	2.13×10^{-3}	1.66	1.00
e	4.37×10^{-2}	3.07×10^{-2}	1.03×10^{-2}	5.49×10^{-3}	4.22	1.00
u	3.12×10^{-2}	1.42×10^{-2}	7.00×10^{-3}	3.91×10^{-3}	2.99	1.00

Table 2: L_1 norms of the difference between exact and computed modified Sod problem results, computed pointwise at $t = 0.2$, for the given variables with the indicated number of points on the unit interval. The prefactor $\mathcal{A}$ and convergence rate σ are least-squares fits to the relation given in Eq. (82). The values of σ close to unity suggest first-order convergence.

	256	512	1024	$\mathcal{A}$	σ
ρ	2.09×10^{-2}	1.08×10^{-2}	5.49×10^{-3}	2.27	0.97
p	6.77×10^{-3}	3.34×10^{-3}	1.80×10^{-3}	0.70	0.96
e	2.21×10^{-3}	1.18×10^{-3}	5.78×10^{-4}	0.24	0.97
u	3.84×10^{-3}	2.05×10^{-3}	9.90×10^{-4}	0.45	0.98

Table 3: L_1 norms of the difference between exact and computed moving-shock problem results, computed pointwise at $t = 0.5$, for the given variables with the indicated number of points on the unit interval. The prefactor $\mathcal{A}$ and convergence rate σ are least-squares fits to the relation given in Eq. (82). The values of σ close to unity suggest first-order convergence.

	$0 < x < 0.1$	$0.1 < x < 0.5$	$0.5 < x < 1$
γ	1.35	1.35	5.0
ρ	2.76470588235	1.0	1.9
e	4.59548599884	2.85714285714	0.131578947368
p	4.44680851064	1.0	1.0
u	1.48327021770	0.0	0.0

Table 4: High-precision initial conditions for the shock-contact problem. This configuration corresponds to a Mach number of 2.0 and an initial shock speed of $u_S = 2.32379000772$, so that the shock hits the material interface at $t = 0.172132593165$.

	$0 < x < x_{RS}$	$x_{RS} < x < x_C$	$x_C < x < x_{TS}$	$x_{TS} < x < 1$
γ	1.35	1.35	5.0	5.0
ρ	2.76470588235	3.95808583566	2.57856549437	1.9
e	4.59548599884	5.23327184191	0.702891658064	0.131578947368
p	4.44680851064	7.24980870307	7.24980870307	1.0
u	1.48327021770	0.930386423194	0.930386423195	0.0

Table 5: High-precision solution for the shock-contact problem at $t = 0.25$. Here, the reflected shock position is $x_{RS} = 0.472708981241754$, the contact position is $x_C = 0.572446778128859$, and the transmitted shock position is $x_{TS} = 0.775299530851478$. The speed of the reflected shock in the laboratory frame is $u_{RS} = -0.350480642253781$, and the speed of the transmitted shock is $u_{TS} = 3.53549118996649$.

	274	549	1099	2199	$\mathcal{A}$	σ
ρ	1.95×10^{-2}	9.61×10^{-3}	4.98×10^{-3}	2.49×10^{-3}	3.61	0.99
p	6.98×10^{-2}	3.09×10^{-2}	1.61×10^{-2}	8.05×10^{-3}	15.6	1.03
e	2.46×10^{-2}	1.11×10^{-2}	5.59×10^{-3}	3.07×10^{-3}	4.66	1.00
u	1.22×10^{-2}	7.01×10^{-3}	3.71×10^{-3}	1.74×10^{-3}	1.80	0.93

Table 6: L_1 norms of the difference between exact and computed shock-contact problem results, computed pointwise at $t = 0.25$, for the given variables with the indicated number of points on the unit interval. The prefactor $\mathcal{A}$ and convergence rate σ are least-squares fits to the relation given in Eq. 82. The values of σ close to unity suggest first-order convergence.

	100	200	400	800	$\mathcal{A}$	σ
$p\ (\times 10^{-6})$	7.15	3.63	1.84	9.19×10^{-1}	675	0.99
ρ	3.30	2.76	1.40	6.98×10^{-1}	133	0.77
$e\ (\times 10^{-3})$	2.12	1.02	5.48	2.68×10^{-1}	196	0.99
u	6.43	3.06	1.64	7.92×10^{-1}	623	1.00

Table 7: L_1 norms of the difference between exact and computed water-air shock tube problem results, computed pointwise, for the given variables with the indicated number of points on the unit interval. Note the normalization factor for the pressure and SIE errors. The prefactor $\mathcal{A}$ and convergence rate σ are least-squares fits to the relation given in Eq. (82). The values of σ close to unity suggest first-order convergence, except for the density, which has an inconsistently low error at the coarsest resolution.
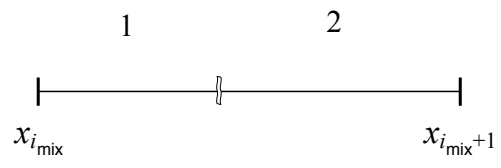
Figure 1: Schematic of the idealized mixed cell, which has material 1 (to the left) separated from material 2 (to the right).
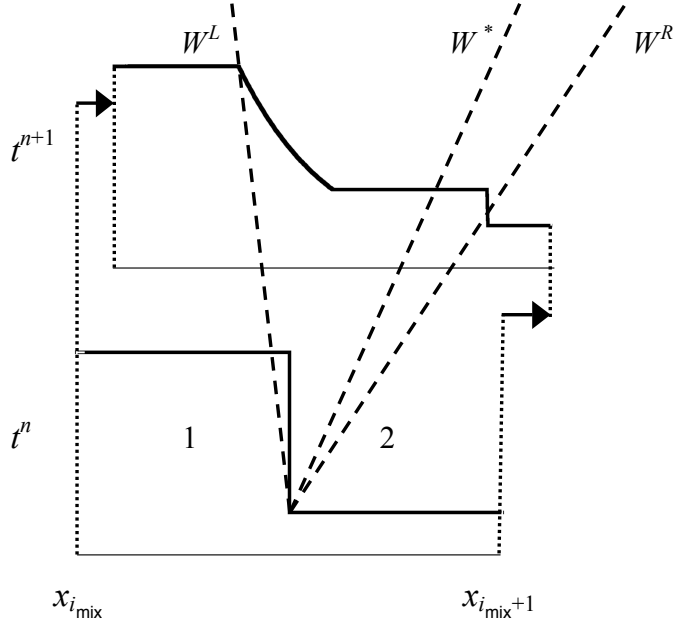
Figure 2: Schematic of the pressure associated with the 1-D Riemann problem used to model the dynamics of the two-material mixed cell. The bottom shows the initial pressure, i.e., at time t^n, of materials 1 (left) and 2 (right), while the top figure is the updated solution, i.e., at time t^{n+1}. The t^{n+1} state exhibits, from left to right, the left t^n value, the leading left-most Riemann wave (W^L, in this case corresponding to a rarefaction fan), the contact discontinuity (W^*), the leading right-most Riemann wave (W^R, in this case corresponding to a shock), and the right t^n quantity.
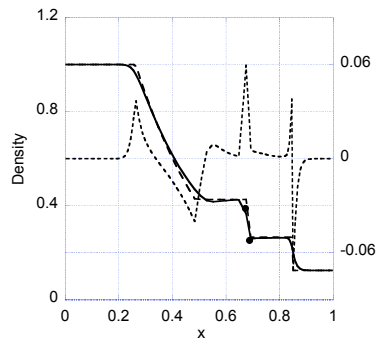
(a) Density
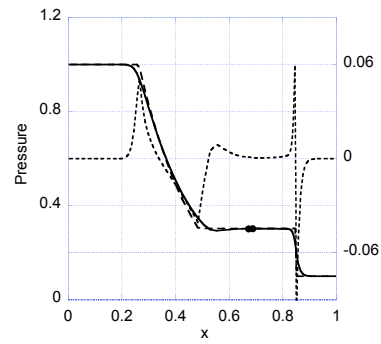
(b) Pressure
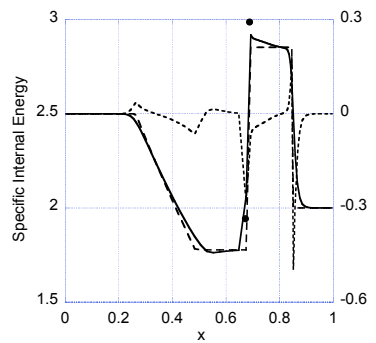
(c) Specific Internal Energy
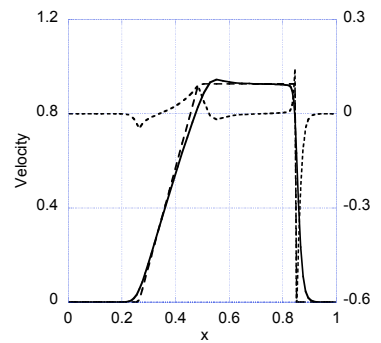
(d) Velocity

Figure 3: Computed results (solid line) for the Sod shock tube problem for 100 zones on $[0, 1]$ at $t = 0.2$. The difference (dotted line) between the computed and exact (dashed line) solutions is plotted against the right ordinate. The values corresponding to the individual materials in the mixed cell are denoted by the symbol $\bullet$.
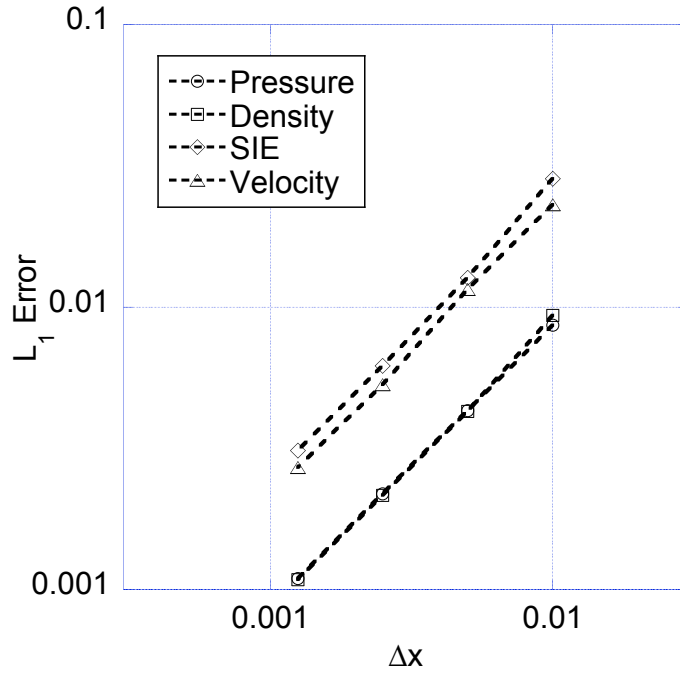
Figure 4: Plot of the L_1 norm of the difference between the computed results and exact solution at $t = 0.2$ for the Sod shock tube problem. The values of the norm for the 100-, 200-, 400-, and 800-zone meshes are shown for the pressure (○), density (□), SIE (◇), and velocity (△). The curve fit parameters corresponding to these data are given in Table 1.
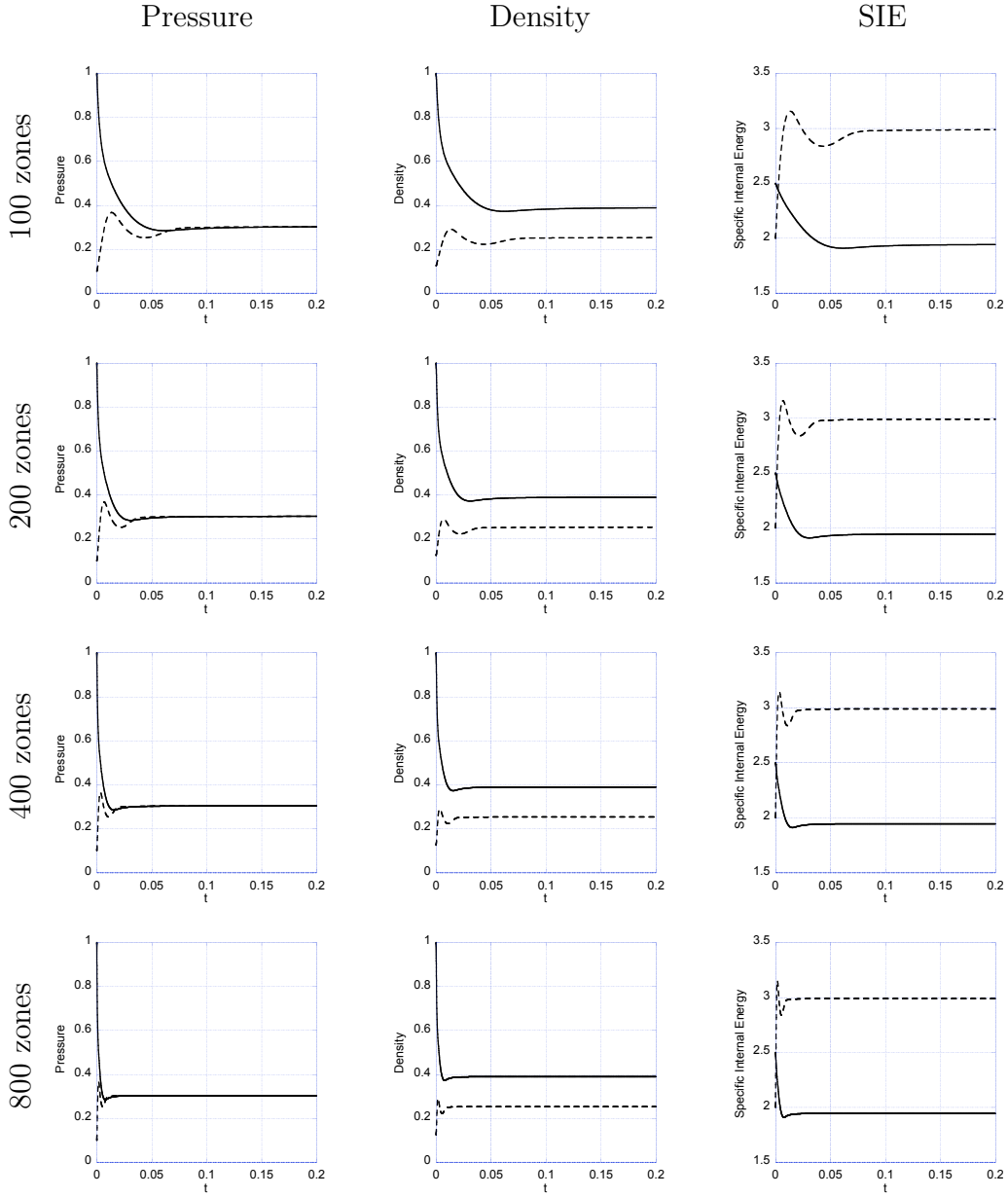
Figure 5: Time-history plots for the Sod shock tube problem of the (from left to right) pressure, the mass density, and SIE of the two materials in the mixed cell, for the (from top to bottom) 100-, 200-, 400-, and 800-cell results. The solid line indicates the left material (material 1) and a dotted line represents the right material (material 2).
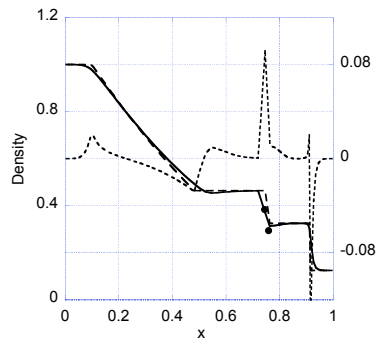
(a) Density
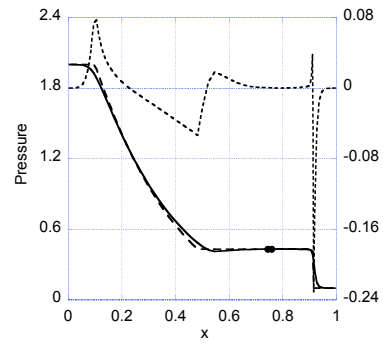
(b) Pressure
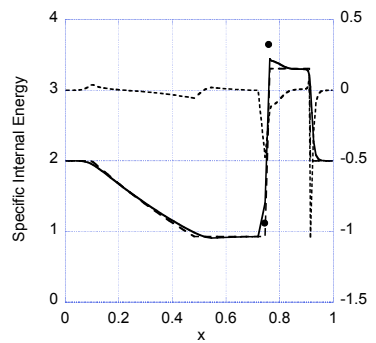
(c) Specific Internal Energy
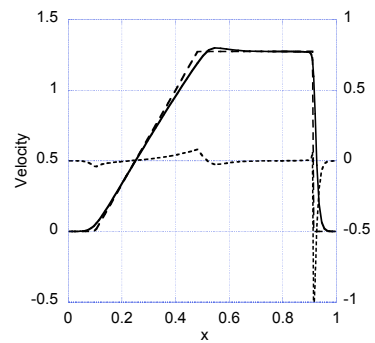
(d) Velocity

Figure 6: Computed results (solid line) for the modified Sod shock tube problem for 100 zones on $[0, 1]$ at $t = 0.2$. The difference (dotted line) between the computed and exact (dashed line) solutions is plotted against the right ordinate. The values corresponding to the individual materials in the mixed cell are denoted by the symbol $\bullet$.
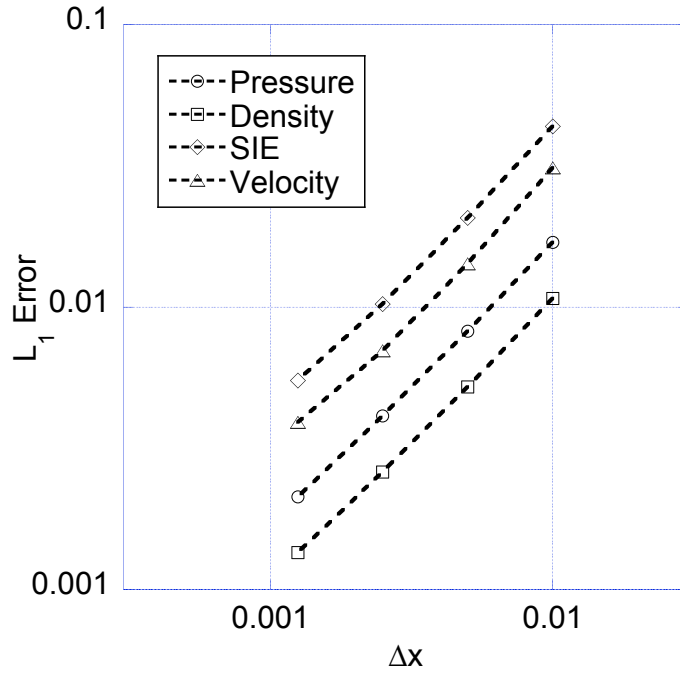
Figure 7: Plot of the L_1 norm of the difference between the computed results and exact solution at $t = 0.2$ for the modified Sod shock tube problem. The values of the norm for the 100-, 200-, 400-, and 800-zone meshes are shown for the pressure ($\circ$), density ($\square$), SIE ($\diamond$), and velocity ($\triangle$). The curve fit parameters corresponding to these data are given in Table 2.

60
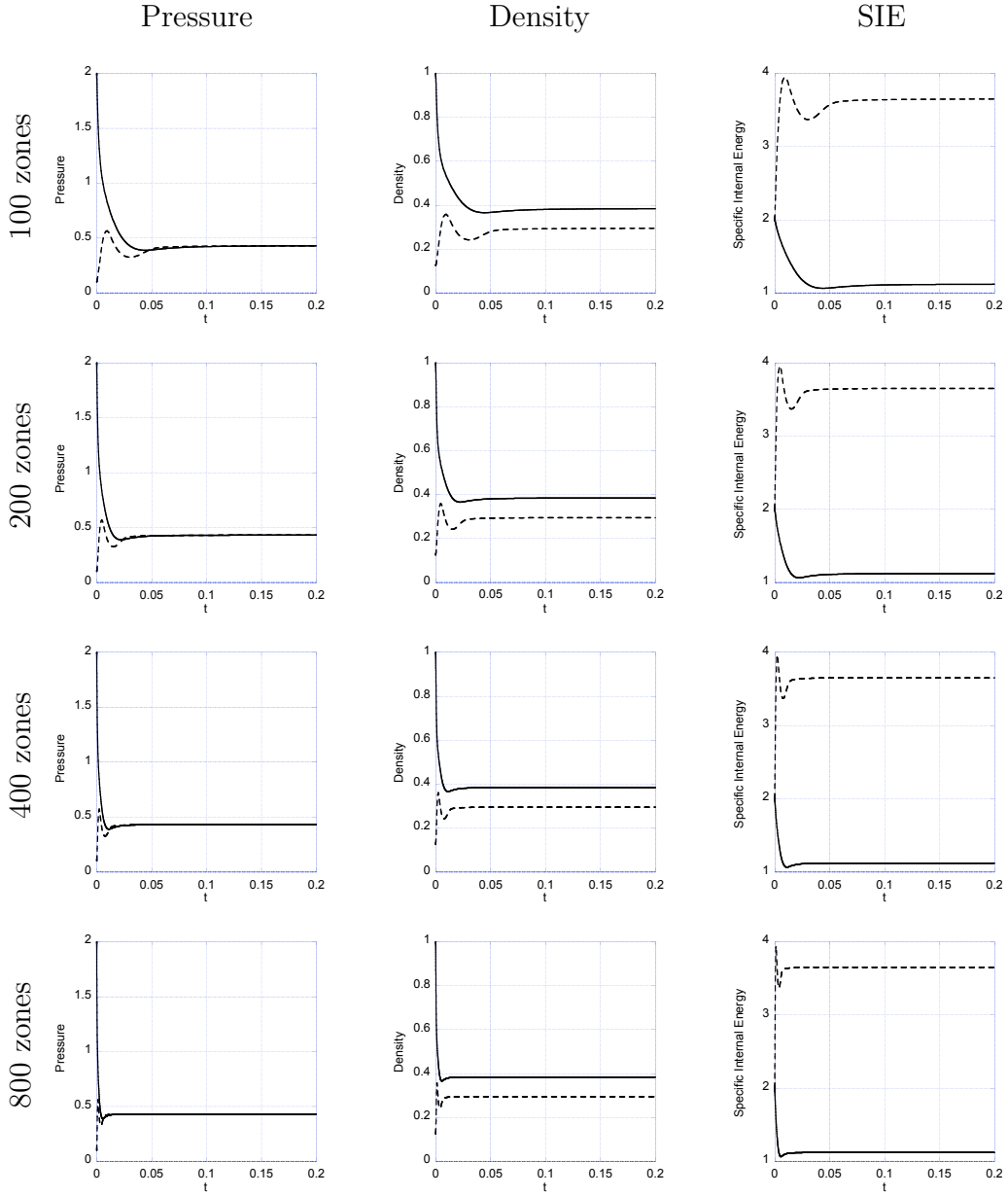
Figure 8: Time-history plots for the modified Sod shock tube problem of the (from left to right) pressure, the mass density, and SIE of the two materials in the mixed cell, for the (from top to bottom) 100-, 200-, 400-, and 800-cell results. The solid line indicates the left material (material 1) and a dotted line represents the right material (material 2).
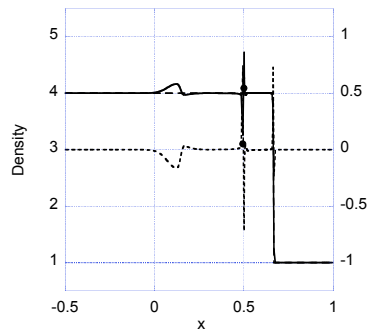
(a) Density
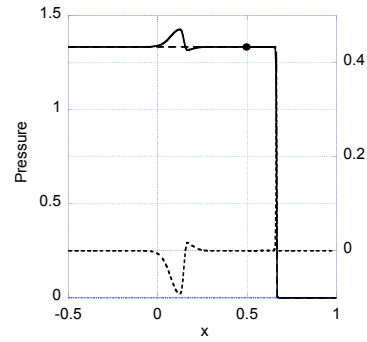
(b) Pressure
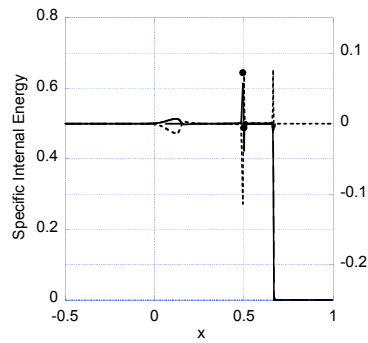
(c) Specific Internal Energy
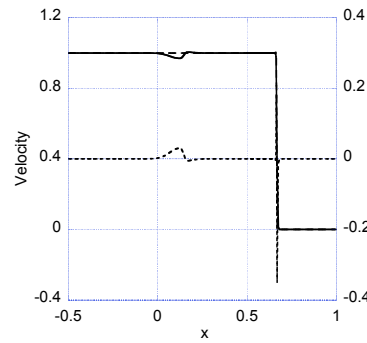
(d) Velocity

Figure 9: Computed results (solid line) for the moving shock for 256 zones on $[0, 2]$ at $t = 0.5$. The difference (dotted line) between the computed and exact (dashed line) solutions is plotted against the right ordinate. The values corresponding to the individual materials in the mixed cell are denoted by the symbol $\bullet$.
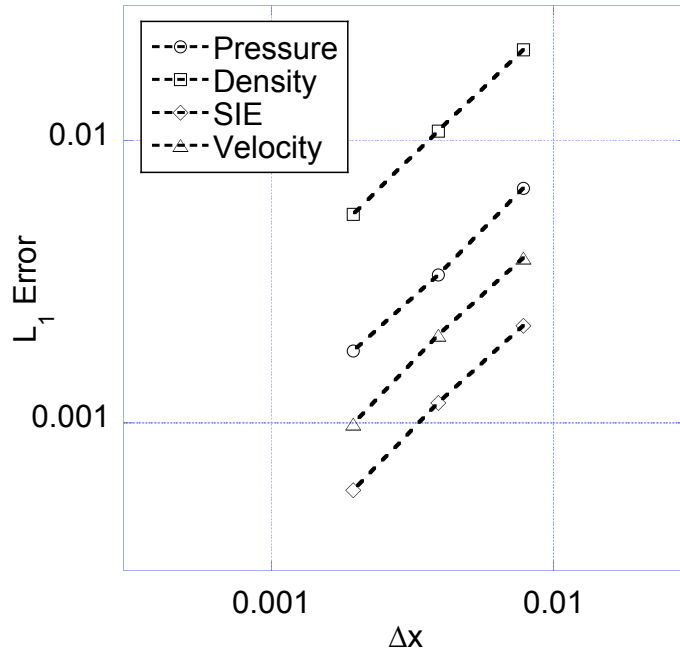
Figure 10: Plot of the L_1 norm of the difference between the computed results and exact solution at $t = 0.5$ for the moving shock problem. The values of the norm for the 256-, 512-, and 1024-zone meshes are shown for the pressure ($\circ$), density ($\square$), SIE ($\diamond$), and velocity ($\triangle$). The curve fit parameters corresponding to these data are given in Table 3.
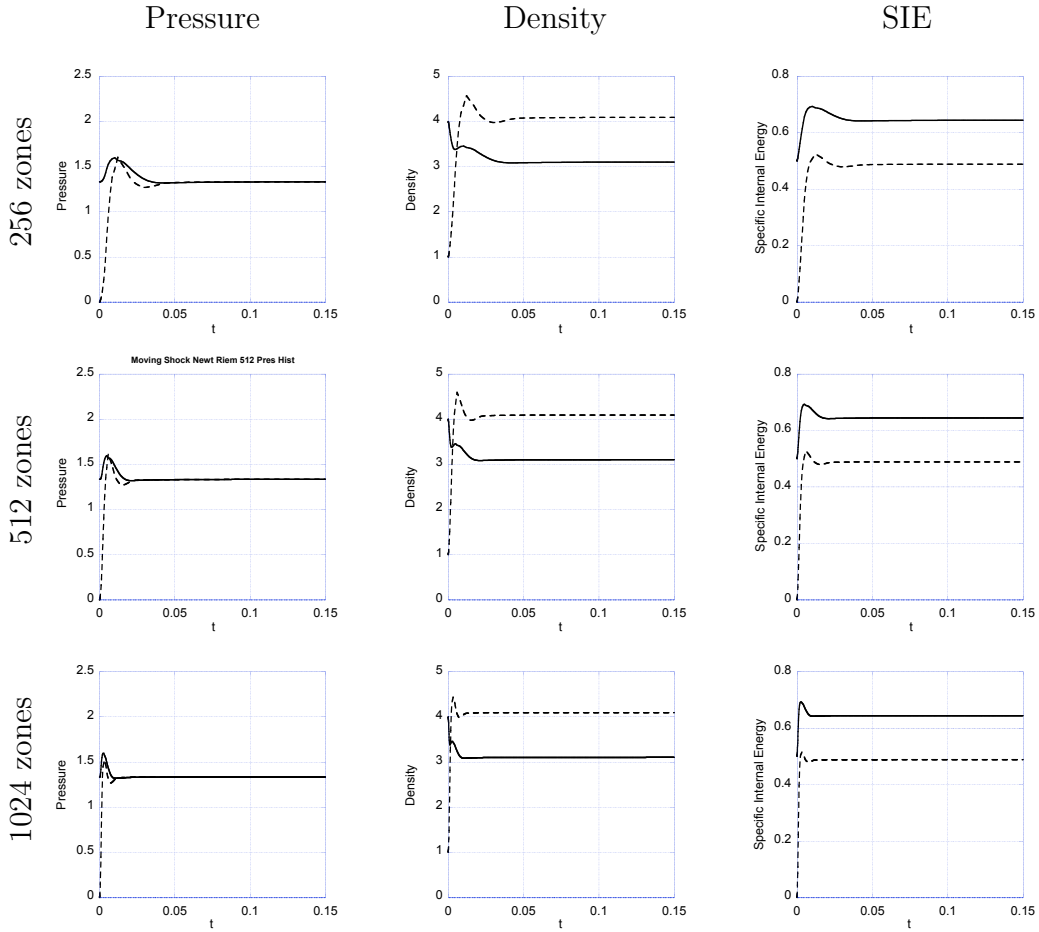
Figure 11: Time-history plots for the moving shock problem of the (from left to right) pressure, the mass density, and SIE of the two materials in the mixed cell, for the (from top to bottom) 256-, 512-, and 1024-cell results. The solid line indicates the left material (material 1) and a dotted line represents the right material (material 2).
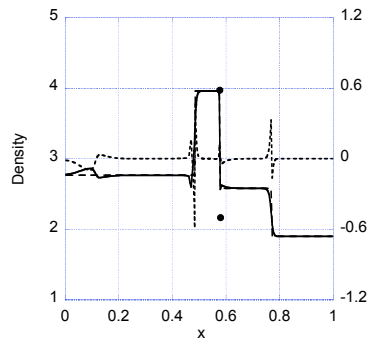
(a) Density
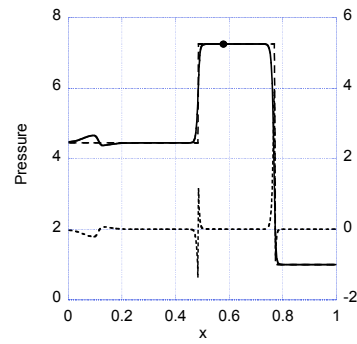
(b) Pressure
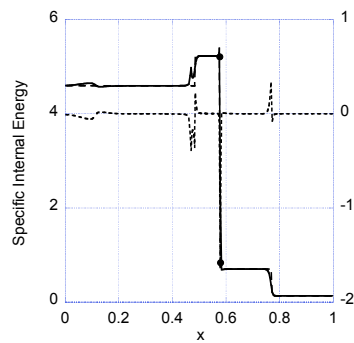
(c) Specific Internal Energy
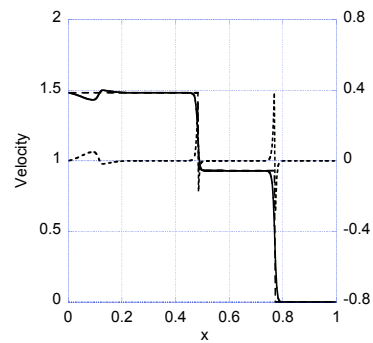
(d) Velocity

Figure 12: Computed results (solid line) for the shock-contact problem at $t = 0.25$ for 274 zones initially on $[-0.37, 1]$. The difference (dotted line) between the computed and exact (dashed line) solutions is plotted against the right ordinate. The values corresponding to the individual materials in the mixed cell are denoted by the symbol $\bullet$.

65
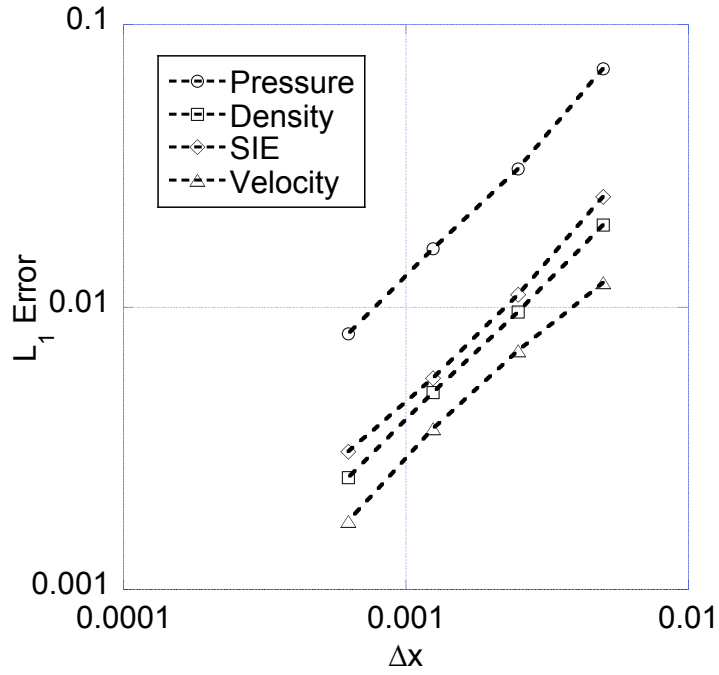
Figure 13: Plot of the L_1 norm of the difference between the computed results and exact solution at $t = 0.25$ for the shock-contact problem. The values of the norm for the 100-, 200-, 400-, and 800-zone meshes are shown for the density ($\square$), pressure ($\circ$), SIE ($\diamond$), and velocity ($\triangle$). The curve fit parameters corresponding to these data are given in Table 6.
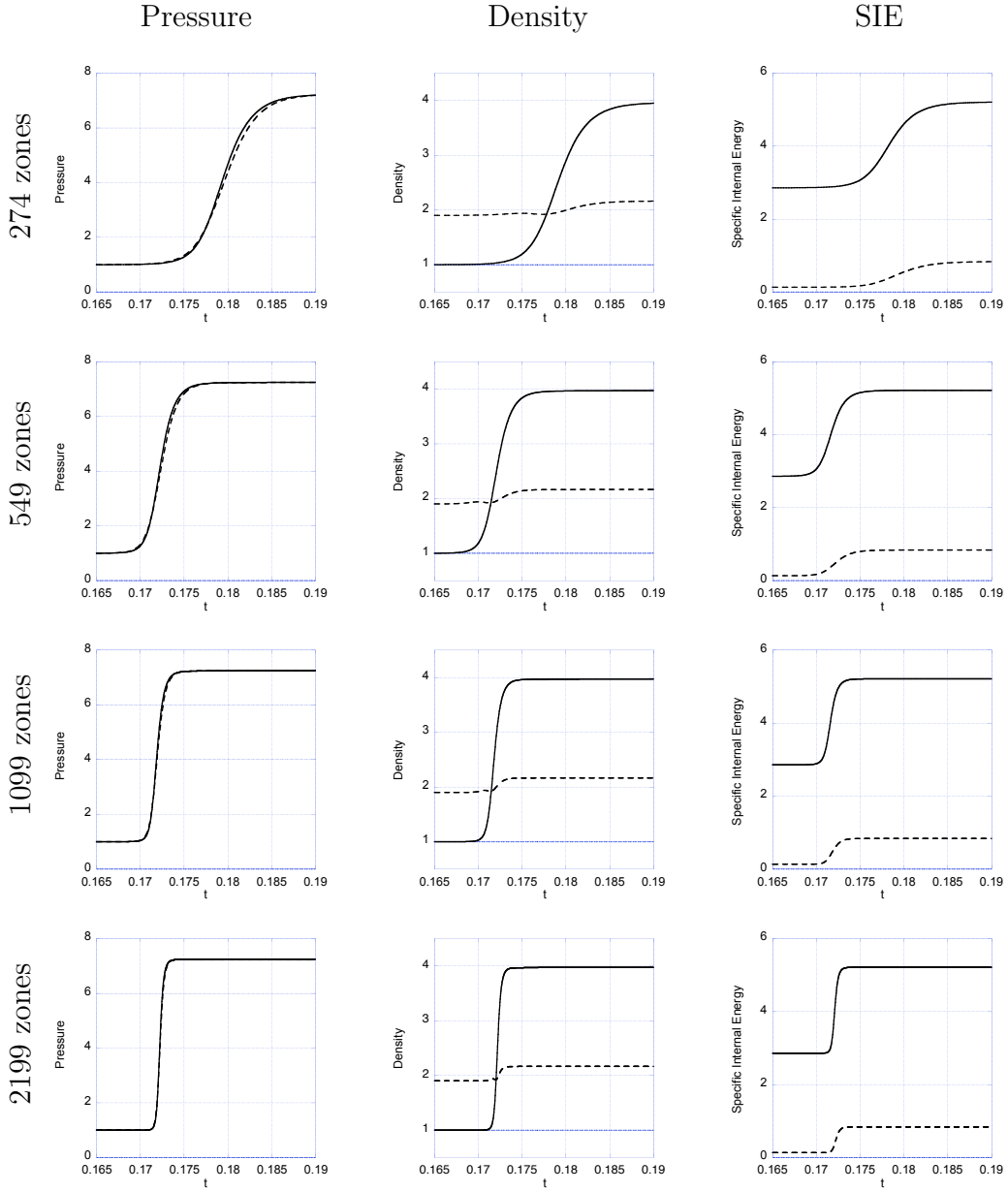
Figure 14: Close-up of time-history plots for the shock-contact problem of the (from left to right) pressure, the mass density, and SIE of the two materials in the mixed cell, for the (from top to bottom) 274-, 549-, 1099-, and 2199-cell results. The solid line indicates the left material (material 1) and a dotted line represents the right material (material 2).
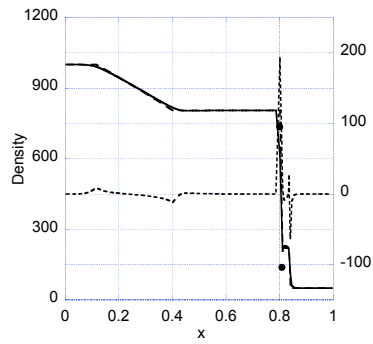
(a) Density
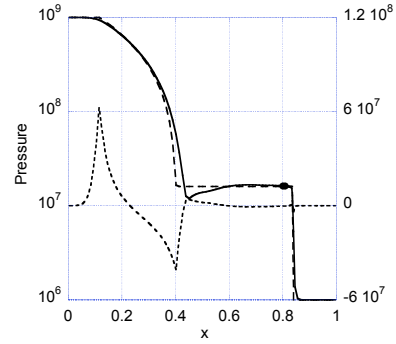
(b) Pressure
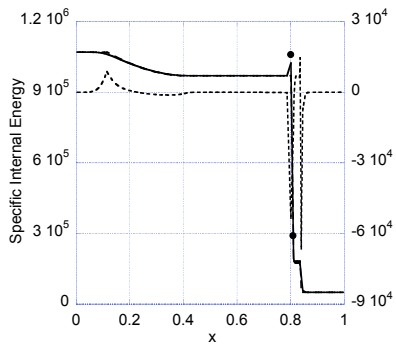
(c) Specific Internal Energy
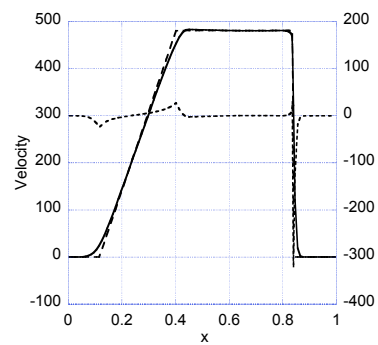
(d) Velocity

Figure 15: Computed results (solid line) for the water-air shock tube problem for 100 zones on $[0, 1]$ at $t = 2.24 \times 10^{-4}$. The difference (dotted line) between the computed and exact (dashed line) solutions is plotted against the right ordinate. The values corresponding to the individual materials in the mixed cell are denoted by the symbol $\bullet$.
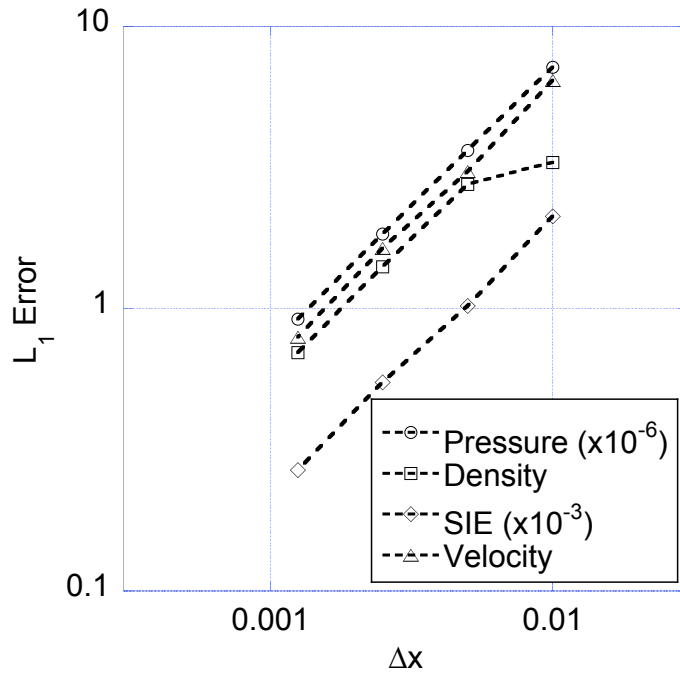
Figure 16: Plot of the L_1 norm of the difference between the computed results and exact solution at $t = 2.24 \times 10^{-4}$ for the water-air shock tube problem. The values of the norm for the 100-, 200-, 400-, and 800-zone meshes are shown for the pressure ($\circ$), density ($\square$), SIE ($\diamond$), and velocity ($\triangle$). In this plot, the values of the pressure error are divided by 10^6 and the SIE errors are divided by 10^3. The curve fit parameters corresponding to these data are given in Table 7.
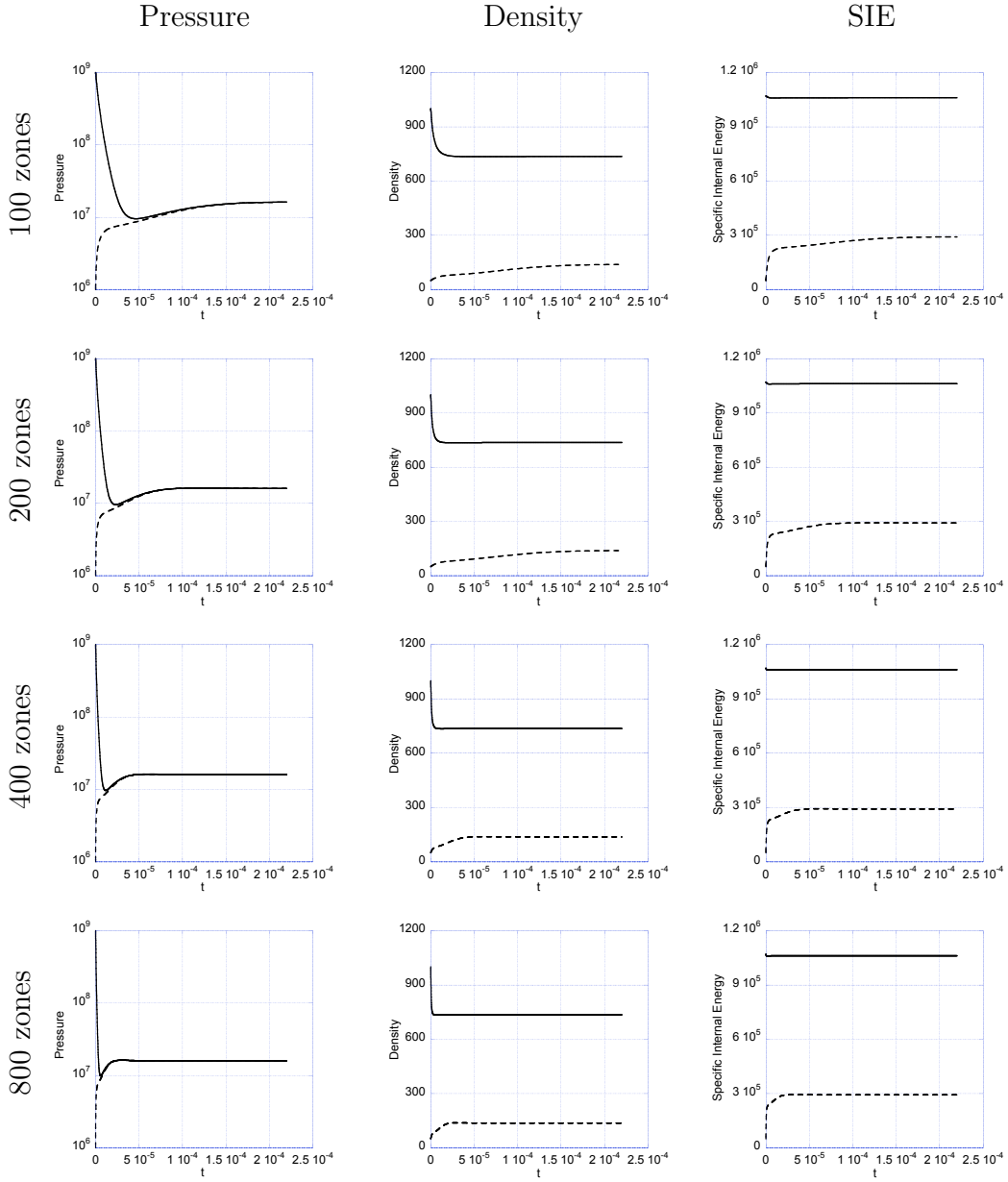
Figure 17: Time-history plots for the water-air shock tube problem of the (from left to right) pressure, the mass density, and SIE of the two materials in the mixed cell, for the (from top to bottom) 100-, 200-, 400-, and 800-cell results. The solid line indicates the left material (material 1) and a dotted line represents the right material (material 2).